Renewable and Sustainable Energy Reviews 31 (2014) 681–707

Contents lists available at ScienceDirect

Renewable and Sustainable Energy Reviews

journal homepage: www.elsevier.com/locate/rser

An overview of ammonia-based absorption chillers and heat pumps

Wei Wu, Baolong Wang, Wenxing Shi, Xianting Li *

Department of Building Science, School of Architecture, Tsinghua University, Beijing 100084, PR China

ARTICLE INFO

Article history:
Received 27 January 2013
Received in revised form
24 September 2013
Accepted 19 December 2013
Available online 22 January 2014

Keywords:
Absorption heat pump
Fluid properties
Subfreezing refrigeration
Heating
Renewable energy
Energy storage

ABSTRACT

The use of ammonia-based working fluids for absorption prevails in a wide range of applications due to the low freezing temperature of the refrigerant and the absence of crystallization as well as the lack of problems under vacuum conditions. This paper presents a comprehensive overview on the use of ammonia-based absorption chillers and heat pumps. The thermodynamic and physical properties of pure ammonia and binary and ternary ammonia mixtures are presented in correlation formulas. Developments and applications in subfreezing refrigeration, heating/domestic hot water, renewable energy utilization, waste heat recovery, thermal energy storage and miniaturization of absorption systems are presented and summarized. In subfreezing refrigeration, the evaporation temperatures for single-stage absorption lie mainly between $-30\,^{\circ}C$ and $-5\,^{\circ}C$, and they can reach as low as $-70\,^{\circ}C$ in advanced absorption systems. Air-source and ground-source absorption heat pumps are suggested for heating/domestic hot water applications in cold regions. For renewable energy uses, ammonia-based solar absorption applications with various working fluids are quite popular, whereas geothermal and biomass energy systems are less studied. In thermal energy storage, ammonia-based working fluids are not advantageous for storage capacity or cycle efficiency, but they prevail for subfreezing energy storage. Additionally, ammonia-based fluids are also attractive options for the miniaturization of absorption systems due to the absence of crystallization.

Contents

* Corresponding author. Tel.: +86 10 62785860; fax: +86 10 62773461.
E-mail address: xtingli@tsinghua.edu.cn (X. Li).

1364-0321/$ - see front matter © 2014 Elsevier Ltd. All rights reserved.
http://dx.doi.org/10.1016/j.rser.2013.12.021

1. Introduction

Originally used for refrigeration, the absorption cycle was invented in the mid-1800s [1] but faded quickly after higher-performance vapor compression refrigeration was introduced. Since the 1960s, absorption technology, especially the absorption refrigeration cycle for air conditioning, has been gradually developed because it primarily consumes low-level heat energy [2] and can play an irreplaceable role in renewable energy use [3,4] and waste heat recovery [5,6]. Finally, the absorption heat pump (AHP) has also drawn attention due to its potential for use in sustainable energy systems providing a high primary energy efficiency and low environmental impact [7,8].

H_2O–LiBr and NH_3–H_2O are the most widely used absorption working fluids [9,10], with the former being more popular due to its higher performance [11]. However, several critical limitations exist for H_2O–LiBr:

- The freezing point of water is 0 °C, and therefore, an H_2O–LiBr AHP that uses water as a refrigerant cannot operate at an evaporation temperature below 0 °C, making it unusable for subfreezing refrigeration [12,13] or heating/domestic hot water (DHW) supplementation in cold regions.
- Crystallization of the H_2O–LiBr solution is quite common, especially when the absorption temperature is high or the evaporation temperature is relatively low, which presents a barrier for air-cooled absorption [14,15].
- High vacuum conditions should be maintained in the system for efficient operation of the H_2O–LiBr system; otherwise, the performance of the absorption cycle would be greatly degraded [16].

These factors render ammonia-based solutions more suitable for adoption as AHP working fluids in certain situations, especially for applications involving subfreezing refrigeration, air-cooled AHPs, AHP heating and DHW, among others. In other applications (i.e., renewable energy utilization, waste heat recovery and thermal energy storage), ammonia-based working pairs have also attracted great attention due to the absence of crystallization and vacuum issues.

Several critical reviews have been published in the literature on the subject of absorption technologies. In 2000, Kang et al. [17] reviewed the performance improvement and temperature lift enhancement of advanced absorption cycles. Srikhirin et al. [18] reviewed different working fluids and cycles for absorption refrigeration in 2001. In 2002, Ziegler [19] defined the state of the art in sorption heat pumping and cooling technologies, including the working fluids and cycles for both absorption and adsorption systems, and Sun et al. [20] presented a review of working fluids for absorption cycles in 2012. However, the previous literature has mainly focused on the development of working fluids and absorption cycles, with most attention centered on air conditioning and refrigeration. No previous review has comprehensively summarized the studies and applications of AHPs using ammonia-based solutions as working fluids, which have special advantages over other fluids. The main objective of this paper is to provide a complete review of ammonia-based AHPs, including both absorption chillers and heat pumps. The thermodynamics and physical properties of different ammonia-based working fluids are covered, which are

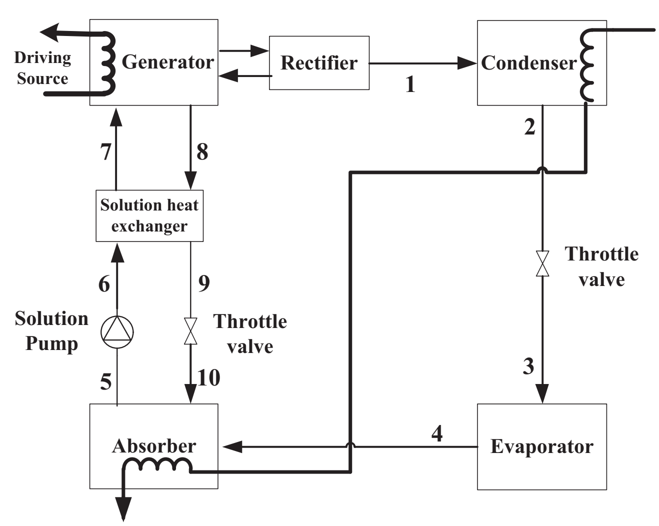


Fig. 1. Schematic of the basic NH_3–H_2O AHP cycle.

Nomenclature

AHP	absorption heat pump
ASAHP	air-source absorption heat pump
ASEHP	air-source electrical heat pump
GSAHP	around-source absorption heat pump
GSEHP	ground-source electrical heat pump
COP	coefficient of performance
CPC	compound parabolic concentrator
DHW	domestic hot water
ECOP	exergy coefficient of performance
GAX	generator absorber heat exchange
LNG	liquefied natural gas
VLE	vapor liquid equilibrium

essential for AHP performance analysis and system simulation. Additionally, various research developments and applications are presented in this work, including subfreezing refrigeration, heating and DHW, renewable energy utilization, waste heat recovery, thermal energy storage and the miniaturization of AHPs.

2. Ammonia-based absorption working fluids

Among ammonia-based absorption working fluids, NH_3–H_2O is the most widely used. Fig. 1 shows a schematic of a basic single-stage AHP cycle that uses NH_3–H_2O as the working fluid. For air conditioning or refrigeration, the coolant passes through the condenser and absorber to remove the heat produced during the absorption and condensation process, and cold water is produced in the evaporator. For heating and DHW, the hot water is heated to the required temperature in the absorber and condenser, and low-grade heat is extracted from the wastewater, ground soil or ambient air by the evaporator. The driving heat source can consist of hot water or steam from boilers, waste hot water in industries or solar energy. Because the boiling points of the refrigerant NH_3 (−77.7 °C) and the absorbent H_2O (100 °C) are relatively similar, a rectifier is necessary in an absorption system to guarantee the purity of the refrigerant vapor exiting the generator (usually no lower than 99.8%); otherwise, the performance will appreciably degrade [21].

2.1. Various ammonia-based working fluids

Increasing interest in absorption heat pumps has led to research on new working fluids. To eliminate the rectifier and simplify the structure of the absorption system, certain alternative working fluids have been studied to a greater extent. The most popular substitutions are the binary ammonia-salt solutions of NH_3–NaSCN and NH_3–$LiNO_3$, which offer the advantages of high solubility in ammonia and no corrosion of steel [22]. Additionally, the boiling point difference between the refrigerant and absorbent is sufficiently large that the generated NH_3 vapor is 100% pure, and the rectifier shown in Fig. 1 can be eliminated [23].

Many studies on binary ammonia-based working fluids have been carried out. Davis et al. [24] tested a number of solutions with different concentrations in the temperature range of −14 °C to 35 °C to select good absorbents for ammonia. The substances shown in Table 1 were tested with positive results. Among the substances tested, $LiNO_3$ appears to offer the highest absorptive value. Chinnappa [25] theoretically and experimentally investigated an intermittent absorption refrigeration cycle employing NH_3–H_2O and NH_3–$LiNO_3$. A simplified approximate expression was presented for the theoretical COP of both working fluids. Best et al. presented tables of flow ratios, the Carnot COP and the enthalpy-based COP under possible operating temperatures and concentrations for NH_3–H_2O [26–29], NH_3–$LiNO_3$ [30–33] and NH_3–NaSCN [34–37] absorption systems used for cooling and heating. Antonopoulos and Rogdakis [38] predicted the hourly performance of solar-driven NH_3–$LiNO_3$ and NH_3–NaSCN absorption systems in the Athens area. Sun [39] simulated the performance of single-stage absorption chillers using NH_3–H_2O, NH_3–$LiNO_3$ and NH_3–NaSCN as working fluids, indicating that NH_3–$LiNO_3$ and NH_3–NaSCN may be suitable alternatives to NH_3–H_2O and that the performance of NH_3–NaSCN is slightly better than that of NH_3–$LiNO_3$. Venegas et al. [40] performed simulations of double-stage and triple-stage absorption systems using NH_3–H_2O, NH_3–$LiNO_3$ and NH_3–NaSCN solutions, with the adoption of a low-temperature driving heat source below 90 °C in both systems. Rivera and Rivera [41] presented the theoretical performance of an intermittent solar absorption refrigeration system operating with an NH_3–$LiNO_3$ mixture and concluded that the overall efficiency of the system was between 0.15 and 0.4 depending on the generation and condensation temperatures. Zhu and Gu [42] conducted a second-law-based thermodynamic analysis of an NH_3–NaSCN absorption system. The COP and exergetic efficiency of the absorption system were calculated under different operating conditions. The results showed that the COP increased with the increase of the heat source temperature and decreased with the increase of the cooling water temperature, but the exergetic efficiency did not show the same trends. Rivera and Best [43] described the experimental results obtained regarding the heat transfer in forced convective boiling for NH_3–H_2O and NH_3–$LiNO_3$ mixtures flowing upward in a uniformly heated vertical tube. Heard and Ayala [44] studied the corrosion of carbon steel and stainless steel in NH_3–$LiNO_3$ for a series of concentration and temperature conditions (from 50 °C to 150 °C). The materials studied were found suitable for the construction of absorption heat pump equipment for this working mixture.

Table 1
Solubility of different substances in ammonia [24].

Substance	NH_4I	NH_4Br	$Ca(NO_3)_2 \cdot 4H_2O$	$Zn(NO_3)_2 \cdot H_2O$	$NaNO_3$
Solubility	Insoluble	Insoluble	Soluble	Sludge formed	Insoluble
Substance	KNO_3	$Pb(NO_3)_2$	$LiNO_3$	$HgNO_3$	$UO_2\ (NO_3)_2 \cdot 6H_2O$
Solubility	Insoluble	Insoluble	Soluble	Pasty mass	Deliquesces
Substance	$Cu(NO_3)_2$	NH_4Cl	$Pb(C_2H_3O_2)_2 \cdot 3H_2O$	KI	NaI
Solubility	Pasty mass	Insoluble	Soft mass	Insoluble	Partly soluble
Substance	NaBr	$AgNO_3$	Lactose	$Sr(NO_3)_2$	
Solubility	Insoluble	Pasty then solid	Insoluble	Insoluble	

In addition, ternary working fluids have also been taken into consideration to overcome the shortcomings of traditional NH_3–H_2O solutions, with NH_3–H_2O–LiBr, NH_3–H_2O–$LiNO_3$ and NH_3–H_2O–hydroxide as the typical representatives.

Compared with the NH_3–H_2O system, the ternary NH_3–H_2O–salt mixture reduces the amount of water in the vapor phase, which implies less rectification or the elimination of rectification. In addition, the operating pressure of the ternary NH_3–H_2O–salt absorption system is much lower. In contrast with the H_2O–LiBr system, the vapor pressure inside the NH_3–H_2O–LiBr system would be non-negative. Mclinden and Radermacher [45] presented a theoretical comparison of the operating performance of NH_3–H_2O and NH_3–H_2O–LiBr absorption heat pumps. The results showed that the ternary solution absorption chillers displayed better performance. Ahlby et al. [46] analyzed the performance of a compression/absorption chiller with an NH_3–H_2O–LiBr ternary solution. Compared with that of the NH_3–H_2O binary system, the COP of the ternary system was better, with a maximum increase of 10%. Wu et al. [47] researched a novel NH_3–H_2O–LiBr absorption refrigeration and air-conditioning system without a solution pump or distillation equipment. The experimental results showed that the vapor pressure of the generator was lower and the COP (with the same mass fraction of ammonia) was 30% higher compared with those of the NH_3–H_2O system.

The heat and mass transfer in the absorber of the NH_3–$LiNO_3$ system are limited by the viscosity of the salt solutions. An alternative to the NH_3–$LiNO_3$ mixture is the NH_3–H_2O–$LiNO_3$ mixture, which shows a higher conductivity and lower viscosity [48]. Bokelmann [49] proposed the addition of water to the binary NH_3–$LiNO_3$ mixture to overcome this drawback. Reiner et al. [50] studied the use of the ternary NH_3–H_2O–$LiNO_3$ mixture for GAX systems as an alternative for the NH_3–H_2O systems. Sathyabhama [51] measured the boiling heat transfer coefficients of NH_3–H_2O, NH_3–H_2O–$LiNO_3$ and NH_3–H_2O–LiBr mixtures. The experimental results indicated that both salts were effective in increasing the heat transfer coefficient of the NH_3–H_2O mixture. For an ammonia mass fraction of 0.30, a high concentration of LiBr gives the highest heat transfer coefficient; for an ammonia mass fraction of 0.25, a high concentration of $LiNO_3$ gives the maximum heat transfer coefficient; and for an ammonia mass fraction of 0.15, both salts are equally effective in increasing the heat transfer coefficient.

The addition of hydroxide to NH_3–H_2O was also proposed to decrease the amount of water in the ammonia vapor. The generation temperature of the NH_3–H_2O–hydroxide system can be reduced relative to that of the NH_3–H_2O system. Reiner and Zaltash [52,53] investigated ternary NH_3–H_2O fluids for absorption cycles to identify the best additives. The results showed that LiBr, LiCl and $LiNO_3$ increase the boiling temperature relative to that of the standard binary solution and that LiOH and KOH decrease it. The authors proposed the addition of hydroxides to the conventional NH_3–H_2O mixture in absorption refrigeration cycles as a method to increase the efficiency and reduce the driving temperature for NH_3–H_2O refrigeration cycles. Steiu et al. [54] conducted a simulation on an NH_3–H_2O–NaOH absorption system using experimental data to calculate the vapor–liquid-equilibrium (VLE) properties, showing that the COP is approximately 20% higher than that of a conventional NH_3–H_2O chiller operating under the same conditions. Via simulation, Balamuru et al. [55] investigated the overall effects of using the working fluid NH_3–H_2O–NaOH on the performance of three absorption cycles. The results indicated that the salting-out effect could lower the generator operating temperature while simultaneously improving the cycle performance. Nevertheless, the salt will tend to salt out the ammonia from the absorber, thereby hindering the absorption, and membrane processes were considered to control the flow of ions from the generator side to the absorber side. Steiu [56] analyzed the technical viability of separating NaOH from NH_3–H_2O–NaOH mixtures using reverse-osmosis membranes. Using an in-series configuration of the modules, the results showed that reverse-osmosis technology is suitable for separating NaOH from the ternary mixtures studied.

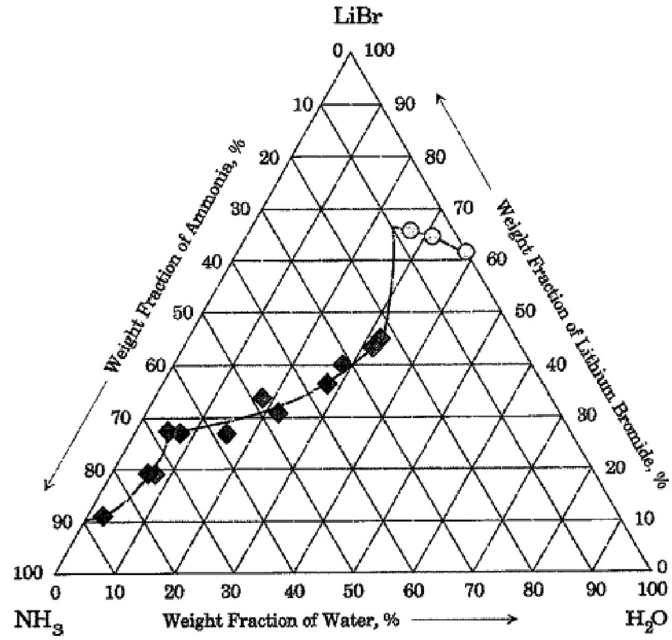


Fig. 2. Ternary diagram of the NH_3–H_2O–LiBr ternary solution [75]. (○ solubility data ◆ triple points)

2.2. Thermodynamic and physical properties

The thermodynamic and physical properties of working fluids are highly important for the studies of absorption chillers and heat pumps. The fitted correlation method defines the property formulas of working fluids by fitting experimental data and both an easily programmable and time-efficient method. The properties of pure ammonia and binary and ternary ammonia mixtures will be presented in this work.

2.2.1. Pure ammonia

The property data for pure NH_3 can be obtained from NIST [57], and the EES [58] software also uses the properties from the NIST. To improve the computation speed, easily programmable and time-efficient property correlations must be achieved. Cleland [59] proposed a property calculation method in the form of curve-fitted equations to achieve higher computation speed. The proposed equations cover R12, R22, R114, R502, NH_3 and a wide range of practical conditions with an accuracy adequate for many practical situations. Sun [39] fitted the phase equilibrium pressure and the specific enthalpies of saturated liquid and vapor NH_3 (expressed in terms of temperature) with source data taken from the ASHRAE handbook [60]. The VLE relations and enthalpy correlations of pure NH_3 provided by Sun and Cleland are listed in Appendix A.1 and A.2.

2.2.2. Binary working fluids

(1) NH_3–H_2O

In the study of the performance of intermittent solar refrigerators, El-Shaarawi and Al-Nimrused [61] used the Gibbs free energy to

develop property equations suitable for use with computers. Schulz [62] published the correlations of NH_3–H_2O for saturated liquid and gas phases over a temperature range of −73 °C to 177 °C and a pressure range of 0.9807 kPa to 2.452 MPa. The calculation results were satisfactory, and the equations were widely used for computational calculation. The property equations of Schulz were given in the form of Gibbs functions. Ziegler et al. [63] extended Schulz′s correlations to a temperature of 227 °C and a pressure of 5 MPa. The values of the specific volume, vapor pressure, enthalpies and equilibrium constants are presented for mixtures in the form of vapor pressure and enthalpy-concentration diagrams. Yokozeki [64] demonstrated a thermodynamically consistent model based on the EOS for refrigerant-absorbent mixtures. The experimental data for the VLE of various binary pairs (including NH_3–H_2O) were analyzed to determine the EOS parameters using the Redlich–Kwong equation, with average absolute relative deviations less than 2% for good-quality VLE data. Mejbri [65] compared three different approaches to formulate the thermodynamic properties of the NH_3–H_2O mixture. Patek et al. [66] presented five equations describing the VLE properties of NH_3–H_2O by fitting critically assessed experimental data using simple functional forms. Sun [39] presented the polynomial equations of PTX and HTX for an NH_3–H_2O mixture with good accuracy. The main thermodynamic and physical property correlations of NH_3–H_2O provided by Schulz, Patek and Sun are presented in Appendix B.1, B.2 and B.3.

(2) NH_3–$LiNO_3$

Aggarwal [67] presented the experimentally thermodynamic property data for 0–70% $LiNO_3$ over a temperature range of −25 °C to 156 °C and up to pressures of 2.2 MPa. The PTX correlations were developed, and the enthalpy of solution, latent heat of vaporization, integral heat of solution, and differential heat of solution were presented in the appropriate tabular and graphical forms. Infante Ferreira [68] presented comprehensive research on the thermodynamic and physical properties of NH_3–$LiNO_3$. The correlations were fitted from experimental data and included the crystallization boundaries, viscosities of solution, heats of solution, densities, heat capacities, thermal conductivities and enthalpies. Using a static method, Libotean et al. [69,70] measured the vapor pressure, density, dynamic viscosity and heat capacity of NH_3–$LiNO_3$ mixtures from 20 °C to 80 °C with ammonia mass fractions ranging from 20% to 60%. The main thermodynamic and physical property correlations of NH_3–$LiNO_3$ provided by Infante Ferreira and Libotean are presented in Appendix C.1 and C.2.

(3) NH_3–NaSCN

Rogdakis and Antonopoulos [71] presented the thermodynamic properties of NH_3–NaSCN. A nomograph was also presented that showed the behavior of the NH_3–NaSCN system in a compact form and allowed direct estimation of its main characteristics. Shrirang [72] experimentally measured several thermo-physical properties of NH_3–NaSCN mixtures at several

Table 2
Characteristics and properties of ammonia-based absorption working fluids.

Working fluid	Advantages and disadvantages	Properties in literature
Binary		
NH_3–H_2O	**Advantages:** Can operate under low evaporation temperatures; Has no crystallization or vacuum problems. **Disadvantages:** Rectifier leads to complex design and large loss.	[39] Equations of PTX and HTX [62] Gibbs free energy, VLE correlation, enthalpy for liquid and gas phase [63] Specific volume, vapor pressure, enthalpies and equilibrium constants [64,66] VLE relations [65] VLE, density, vaporization heat
NH_3–$LiNO_3$	**Advantages:** Rectifier can be eliminated; High solubility in ammonia and no corrosion to steel; Lower driving temperature and better performance than NH_3–H_2O. **Disadvantages:** Performance is limited by high viscosity of salt solutions.	[67] PTX, vaporization heat, integral and differential heat of solution; [68] VLE, enthalpy, density, viscosity, thermal conductivity, specific heat, crystallization line; [69,70] vapor pressure, density, dynamic viscosity, and heat capacity
NH_3–NaSCN	**Advantages:** Rectifier can be eliminated; High solubility in ammonia and no corrosion to steel; Lower driving temperature and better performance than NH_3–H_2O. **Disadvantages:** Crystallization may occur at low evaporation temperatures.	[22] Solubility, density, vapor pressure, viscosity, thermal conductance, heat of solution and heat Capacity; [68] VLE, enthalpy, density, viscosity, thermal conductivity, specific heat, crystallization line; [72] VLE, density, dynamic viscosity, isobaric heat capacity
Ternary		
NH_3–H_2O–$LiNO_3$	**Advantages:** Higher heat transfer coefficient and lower viscosity than binary mixtures; Lower vapor pressure and lower water content in the refrigerant vapor. **Disadvantages:** Boiling temperature is higher than binary mixtures	[69] VLE characteristics; [70] Density, dynamic viscosity, and heat capacity
NH_3–H_2O–LiBr	**Advantages:** Higher heat transfer coefficient and better performance than binary mixtures; Lower vapor pressure and lower water content in the refrigerant vapor. **Disadvantages:** Boiling temperature is higher than binary mixtures	[47,73,74,76] VLE characteristics; [75] Triple line and crystallization line
NH_3–H_2O–XOH	**Advantages:** Higher efficiency and lower driving temperature than NH_3–H_2O cycles; Lower vapor pressure and lower water content in the refrigerant vapor. **Disadvantages:** Salt will tend to salt out ammonia from the absorber and lead to a bad absorption process.	[78,79] VLE characteristics; [80] Heat capacity and density

temperatures: density from −3.8 °C to 77.8 °C, dynamic viscosity from −3.4 °C to 96.4 °C, isobaric heat capacity from 3 °C to 91 °C and VLE data from −20 °C to 120 °C. All properties were measured in a range of compositions from 35% to 90% by ammonia mass fraction, were correlated as a function of temperature and composition using empirical equations and were compared with the literature values. Infante Ferreira [68] presented property correlations of NH_3–NaSCN fitted from experimental data. The main thermodynamic and physical property correlations of NH_3–NaSCN provided by Infante Ferreira and Shrirang are presented in Appendix D.1 and D.2.

2.2.3. Ternary working fluids

(1) NH_3–H_2O–LiBr
Peters et al. [73] conducted an experimental investigation of the VLE characteristics of a NH_3–H_2O–LiBr ternary solution at temperatures ranging from 30 °C to 150 °C and pressures ranging from 0.1 MPa to 1.5 MPa. The salt concentration in the liquid phase was chosen from the range of 5–60% of the mass ratio of LiBr in pure water. Later, Peters et al. [74] developed a quasi-chemical reaction model to correlate the VLE data for the NH_3–H_2O–LiBr system at temperatures ranging from 30 °C to 200 °C and at pressures up to 2.0 MPa. The activities of the various components in the liquid phase were modeled using the NRTL equation. This group also measured the solid–liquid equilibrium at ambient pressure and the solid–liquid–vapor equilibrium at T=30 °C in the NH_3–H_2O–LiBr system. Fig. 2 presents a ternary phase diagram of the system at T=30 °C, showing its triple line and crystallization line [75]. Crystallization may occur in the NH_3–H_2O–LiBr system, but the limit concentration of LiBr will be higher than in the H_2O–LiBr system at the same solution temperature. Wu et al. [47,76] carried out an experimental investigation of the VLE characteristics of an NH_3–H_2O–LiBr ternary solution over a temperatures range of 15–85 °C and pressures up to 2.0 MPa. The LiBr concentration of the solution was chosen in the mass ratio range of 5–60% LiBr in pure water. The PTX relations were presented in the form of tables and graphs.

(2) NH_3–H_2O–$LiNO_3$
Using a static method, Libotean et al. [69] measured the vapor pressure of NH_3–H_2O–$LiNO_3$ mixtures from 20 °C to 80 °C for ammonia mass fractions ranging from 20% to 60%. This group also measured the density, dynamic viscosity and heat capacity of NH_3–H_2O–$LiNO_3$ mixtures between 20 °C and 80 °C at 1.8 MPa using a vibrating-tube densimeter, a piston-style viscometer and a heat flux Calvet-type calorimeter, respectively [70]. The measured data were correlated as a function of temperature and composition using simple polynomial equations. The VLE relations and property correlations of NH_3–H_2O–$LiNO_3$ provided by Libotean are listed in Appendix E.1.

(3) NH_3–H_2O–hydroxide
The built-in thermodynamic property data in the ASPEN software can be applied for NH_3–H_2O–hydroxide mixtures [77], and Balamuru et al. [55] numerically solved the model of an NH_3–H_2O–NaOH absorption cycle using this program. Brasset al. [78] used a static method to obtain the VLE data for NH_3–H_2O–NaOH and NH_3–H_2O–KOH absorption systems at temperatures of 30 °C and 45 °C, pressures ranging from 0.1 MPa to 1.3 MPa and salt concentrations in the range of 2–60% in water. Salavera et al. [79] measured the VLE data of NH_3–H_2O–NaOH and NH_3–H_2O–KOH mixtures from 20 °C to 80 °C using a static method; they also studied the heat capacity and density between 20 °C and 80 °C at a constant pressure of 1.8 MPa for both solutions. All of the experimental results were well correlated with the temperature and mass concentration using analytical polynomial equations [80]. The VLE relations and property correlations of NH_3–H_2O–NaOH and NH_3–H_2O–KOH provided by Salavera are listed in Appendix E.2.

The advantages and disadvantages of ammonia-based absorption working fluids and their thermodynamic and physical properties in the published literature are summarized in Table 2. It is clear that the properties of ternary working fluids have been researched to a much lesser degree compared with those of binary mixtures.

3. Subfreezing refrigeration

In the refrigeration field, many applications exist that require cooling effects at low temperatures, such as freezing processes, ice-making and cold storage. In principle, ammonia-based absorption chillers could operate at temperatures well below the usual air-conditioning temperatures, which may be useful for sub-zero refrigeration applications and represents one of the main advantages of ammonia-based over water-based working fluids. Based on absorption cycles, subfreezing refrigeration is divided into basic absorption refrigeration and advanced absorption refrigeration. The advanced cycles are commonly used to obtain lower refrigeration temperatures than those of the basic absorption cycles.

3.1. Basic absorption refrigeration

Lazzarin et al. [81] studied the possibility of an air-cooled NH_3–H_2O refrigerator and compared the results with the experimental data supplied by a manufacturer. Clerx and Trezek [82] performed a computer-aided thermodynamic analysis of a solar-assisted NH_3–H_2O absorption ice-making unit at subfreezing evaporator conditions for various ranges of operation parameters, three climatic locations and four solar collector types and compared the performance and cost of different systems. Moreno-Quintanar [83] developed a solar absorption refrigeration system for ice production using NH_3–$LiNO_3$ and NH_3–$LiNO_3$–H_2O as the working fluids. The system was designed to produce up to 8 kg of ice per day, and evaporation temperatures as low as −8 °C were obtained for a time period of 8 h. Tests indicated that with the ternary mixture, the COP could reach a value up to 24% higher than that of the binary mixture, varying from 0.066 to 0.093. Colonna and Gabrielli [84] presented a thermodynamic study of tri-generation configurations, with NH_3–H_2O absorption refrigeration plants

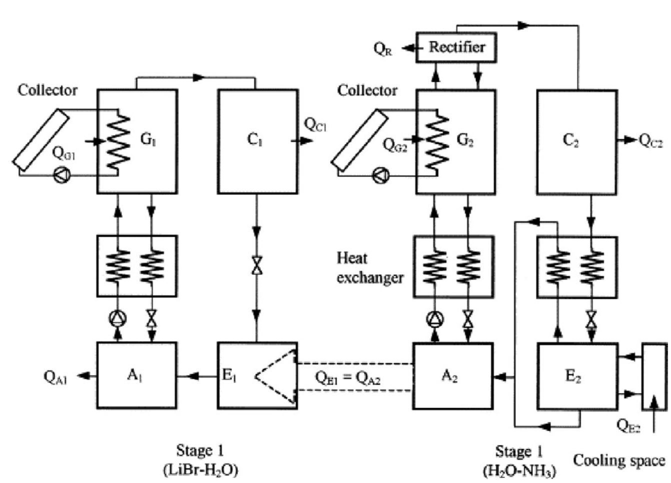


Fig. 3. Double-stage cascade dual-fluid absorption refrigeration system [87].

coupled to internal combustion engines or turbo-generators to simultaneously provide electricity and refrigeration at low temperatures. Bassols et al. [85] studied the combination of a NH_3–H_2O absorption refrigeration with a co-generation plant for low-temperature cooling between −15 °C and −55 °C for the food industry.

3.2. Advanced absorption refrigeration

Realistically, a large number of deep-freezing demands at temperatures below −20 °C are presented in many industrial processes, including the food industry, the pharmaceutical industry and in chemical engineering [86]. Advanced absorption cycles could be applied to meet the low-temperature demand for such applications as the double-stage cascade cycle, the double-stage absorption cycle and hybrid absorption/compression cycle.

In the double-stage cascade cycles, the evaporator of the first stage produces cooling water, which is circulated in the absorber and condenser of the second stage. Double-stage cascade systems can be used for the production of notably low temperatures with the use of moderate generation temperatures in the first stage. Kaushik and Kumar [87] presented a thermodynamic assessment of a double-stage cascade dual-fluid absorption refrigeration system using H_2O–LiBr and NH_3–H_2O as the working fluids in the first and second stage, respectively, as shown in Fig. 3. Both stages were assumed to operate with hot water available from separate solar collectors. The results showed that the COP of a double-stage cascade system is lower than that of a single-stage system; however, the second stage can be operated at lower generation temperatures [88]. This group also investigated a double-stage cascade absorption system with NH_3–H_2O and NH_3–$LiNO_3$ and observed that the COP is higher for NH_3–$LiNO_3$ than for NH_3–H_2O, in both the single-stage and double-stage cascade absorption systems, especially at higher generation temperatures [89]. Rogdakis and Antonopoulos [90] studied a NH_3–H_2O cascade absorption refrigeration system, which can be used to produce refrigeration temperatures as low as −70 °C. For an ambient temperature of 10 °C, the theoretical COP ranged from 0.20 to 0.65 when the lowest temperatures ranged from −70 °C to −30 °C. Fernández-Seara [91] analyzed a cascade refrigeration system that used a compression cycle in the low-temperature

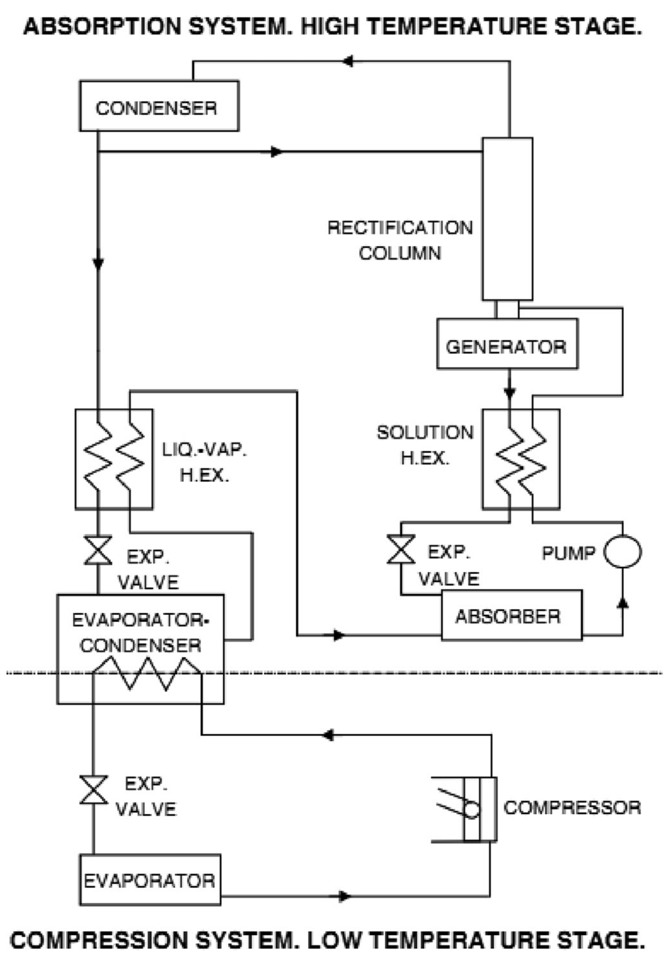


Fig. 4. Schematic of the compression–absorption cascade refrigeration system [91].

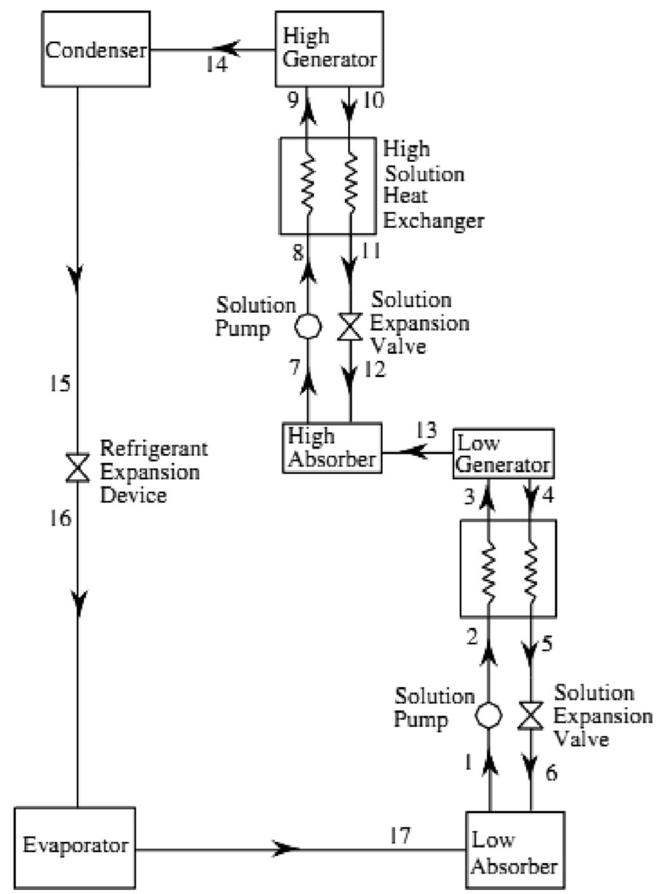


Fig. 5. Schematic of the double-stage absorption refrigeration system [92].

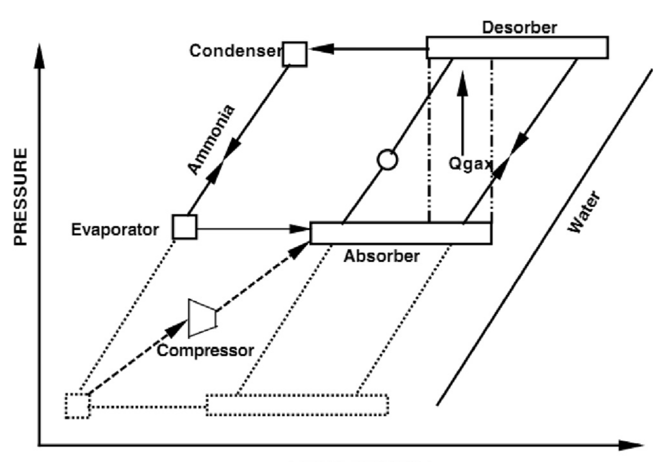


Fig. 6. Concept of absorption/compression GAX cycle [94].

stage and an absorption cycle in the high-temperature stage to generate cooling at low temperatures. For the refrigerants, CO_2 and NH_3 were considered in the compression stage and NH_3–H_2O was considered in the absorption stage. Both stages share a heat exchanger, which operates simultaneously with the condenser of the compression system and the evaporator of the absorption system, as shown in Fig. 4.

In the double-stage cycles (also referred to as the half-effect cycles), the vapor created in the generator of the low-pressure stage enters the absorber of the high-pressure stage, as shown in Fig. 5 [92]. The double-stage configuration is able to operate at considerably lower generation and evaporation temperatures than the single-stage cycle system but at the cost of a lower COP. The double-stage H_2O–NH_3 absorption cycle is commonly used for refrigeration with low evaporation temperatures [20]. Venegas et al. [40] simulated double-stage absorption systems driven by low-temperature heat at low evaporation temperatures. The results showed that the NH_3–$LiNO_3$ solution operated with a COP of 0.32, the H_2O–NH_3 operated with a COP of 0.29 and the NH_3–NaSCN operated with a COP of 0.27 when the evaporation, condensation and generation temperatures were −15 °C, 40 °C and 90 °C, respectively. In this research, the evaporation temperatures ranged between −40 °C and 0 °C. Arzoz et al. [93] reported the successful operation of a 3-kW double-stage $LiNO_3$–NH_3 absorption machine using low-temperature solar heat. A COP of 0.27 was obtained with a heat source temperature of 90 °C for an evaporation temperature of −15 °C and a condensation temperature of 45 °C.

Absorption/compression cycles can be also used for low-temperature refrigeration applications, and absorption/compression coupled with GAX (generator absorber heat exchange) is able to achieve better performance. The concept of an absorption/compression GAX cycle is illustrated in Fig. 6 [94]. The absorber pressure is able to maintain the same pressure as that of the standard GAX cycle, whereas the evaporator pressure becomes lower than the absorber pressure, leading to a low evaporation temperature. Kumar and Udayakumar conducted simulation studies on an absorption/compression GAX cycle using NH_3–H_2O, and the de-gassing range of the cycle was optimized for maximum COP [95]. This group also studied the effect of the compressor pressure ratio on an absorption/compression GAX cooler with a capacity of 3.514 kW. The low-side pressure ratio of the cycle was optimized for an optimum COP [94]. Kang et al. [96] observed that an evaporation temperature of −50 °C can be obtained from the absorption/compression GAX cycle with a COP of 0.58, which is much higher than that of the conventional vapor compression cycle for low-temperature applications.

The subfreezing refrigeration systems with different absorption cycles using various working fluids are summarized in Table 3. For single-stage absorption systems, the evaporation temperatures lie primarily in the range of −30 °C to −5 °C and can reach as low as −70 °C for advanced absorption refrigeration systems.

4. Heating and domestic hot water

Most of the research on ammonia-based absorption systems has focused on cooling and refrigeration; however, a gas-fired absorption chiller can also produce hot water for heating and DHW. In this situation, the absorption cycle acts as a gas boiler rather than a heat pump cycle. From an energy conservation point of view, the AHP cycle should be adopted to provide heating and DHW due to its high primary energy efficiency. However, when operating in heat pump mode, the crystallization of H_2O–LiBr due to the higher condensation and absorption temperatures may be a

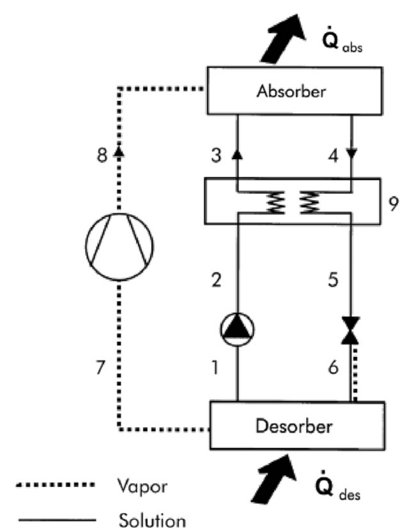


Fig. 7. Schematic of the compression/absorption heat pump [98].

Table 3
Summary of subfreezing refrigeration for different absorption cycles.

Cycle	Evaporation temperature	COP	Working fluid	Reference
Single-stage	−30 to 5 °C	0.25–0.55	NH_3–H_2O	Lazzarinet al. [81]
	−18 to 3 °C	0.49–0.58	NH_3–H_2O	Clerx and Trezek [82]
	−8 °C	Solar COP 0.066–0.093	NH_3–$LiNO_3$ NH_3–$LiNO_3$–H_2O	Moreno-Quintanar [83]
	−10 °C	0.60	NH_3–H_2O	Colonna and Gabrielli [84]
	−30 to 10 °C	/	NH_3–H_2O	Bassolset al. [85]
Double-stage cascade	−20 to 0 °C	0.17–0.31	Stage 1: H_2O–LiBr Stage 2: NH_3–H_2O	Kaushik and Kumar [87,88]
	−20 to 0 °C	Approx. 0.25	NH_3–H_2O NH_3–$LiNO_3$	Kaushik and Kumar [89]
	−70 to −30 °C	0.20–0.65	NH_3–H_2O	Rogdakis and Antonopoulos [90]
	−45 °C	0.25	Stage 1: NH_3–H_2O Stage 2: CO_2/NH_3	Fernández-Seara [91]
Double-stage	−15 to 0 °C	0.32 0.29 0.27	NH_3–$LiNO_3$ H_2O–NH_3 NH_3–NaSCN	Venegas et al. [40]
	−15 °C	0.27	NH_3–$LiNO_3$	Arzoz et al. [93]
Absorption/compression	−10 °C	1.00	NH_3–H_2O	Kumar and Udayakumar[94,95]
	−50 °C	0.58	NH_3–H_2O	Kang et al. [96]

problem, which suggests the use of ammonia-based solutions as potential alternative working fluids. Additionally, the low freezing point of NH_3 makes the ammonia-based fluids promising for air-source absorption heat pumps (ASAHP) and ground-source absorption heat pumps (GSAHP), especially in cold regions.

4.1. Compression/absorption heat pump (CAHP)

The CAHP systems had been previously proposed for heat pump applications, which were regarded as potential alternatives to the conventional vapor compression and vapor absorption systems due to their unique features [97]. A typical schematic of a CAHP is shown in Fig. 7 [98]. The evaporator and the condenser are replaced by a generator (desorber) and an absorber in a process also known as the resorption/compression cycle [99]. The desorber operates at low pressure and removes heat from the ambient fluid, and during absorption, the absorber releases the heat to heat the space. In this configuration, the system can be operated at a much lower pressure and a higher required temperature of the hot water compared with the conventional vapor compression heat pump. Consequently, CAHP systems are suitable for large temperature variations and high-temperature applications [100].

Tariquea and Siddiqui [101] carried out a performance study and an economic analysis of a CAHP system with an NH_3–NaSCN solution and compared it with that of pure NH_3 in the compression cycle under various operating conditions. The performance, specific compressor displacement, electricity costs and capital costs were studied with the pressure ratios and heating temperatures treated as the variables. The capital costs and operating costs of the compressors with NH_3–NaSCN were highly reduced compared with those of the compression cycle. The performance of NH_3–NaSCN in the combined cycle for a fixed value of the heating temperature was nearly 30–60% higher than that in the compression cycle.

Hultén and Berntsson [98] compared the COP of an NH_3–H_2O CAHP and isobutene compression heat pump for various heating applications with a specified investment level. Typical industrial or district heating cases were chosen to study the impact of different temperature lifts and the glide of the heat sink and source. The results showed that the CAHP displayed a 12% better performance than the compression heat pump when the glide of the sink and source increased to 20 °C. Certain COP-increasing design parameters for further study were brought forward for the CAHP. In another work, this same group modified the CAHP and increased the COP by 10%. The improved design displayed a lower optimal absorber glide and reduced solution heat exchanger sizes. The performance of the CAHP was studied for five heating cases and was compared with that of a two-stage compression heat pump

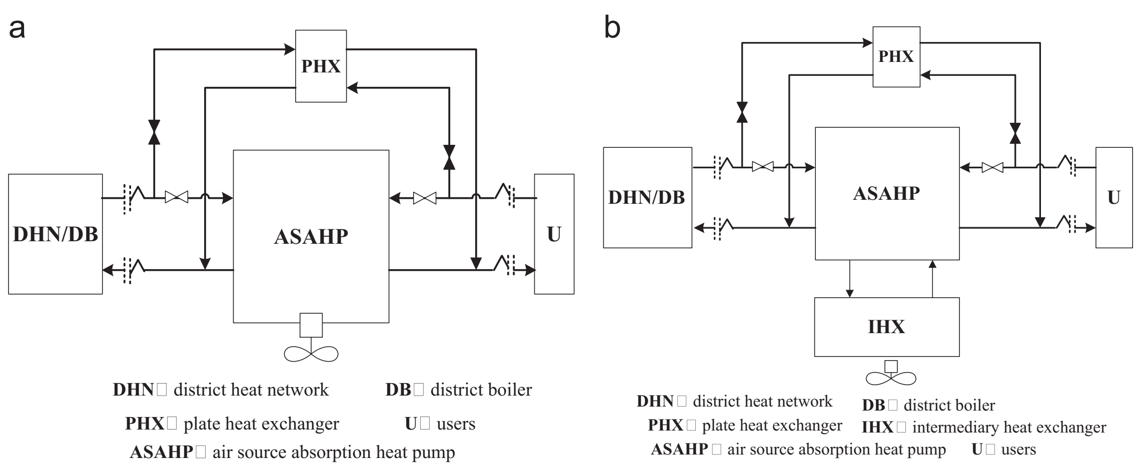


Fig. 8. Schematic of the ASAHP combined with conventional heating systems [103].

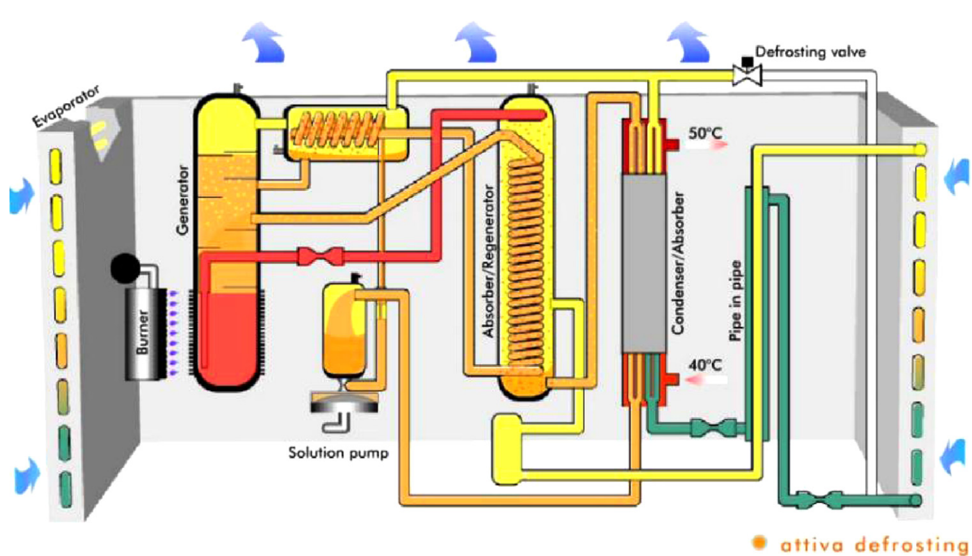


Fig. 9. Gas-fired ASAHP [104].

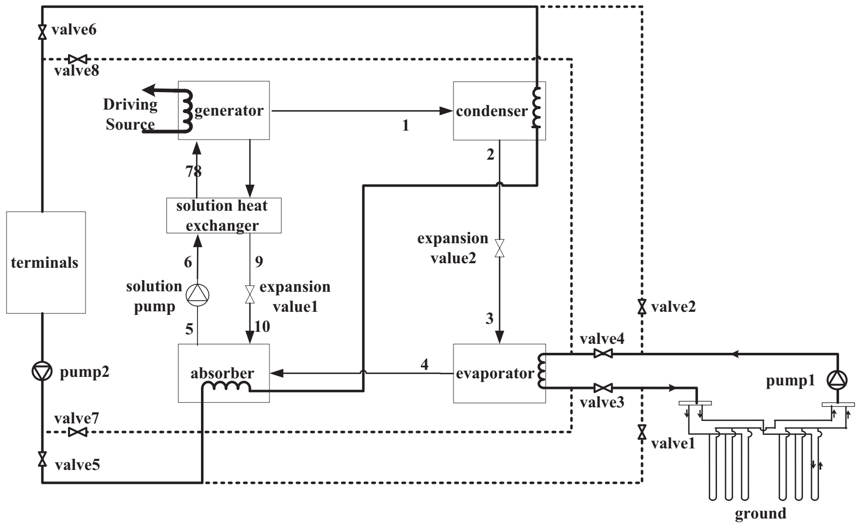


Fig. 10. Schematic of the GSAHP [105].

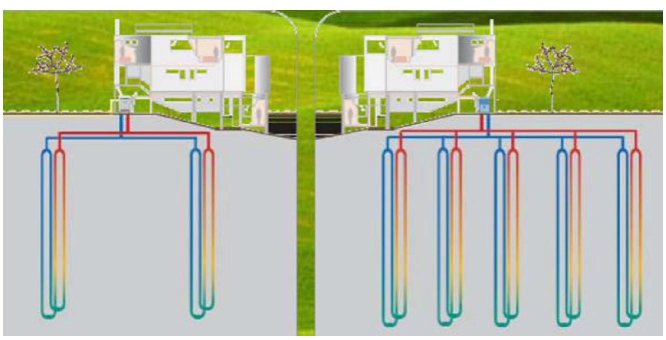


Fig. 11. Gas-fired GSAHP [104].

based on an approximately equal investment cost. When both the sink and the source temperature glide were large (>20 °C), the CAHP yielded superior performance [102].

4.2. Air/ground source absorption heat pump (ASAHP/GSAHP)

Recently, the ASAHP and GSAHP were applied for heating and domestic hot water in both experimental studies and in real products. Li et al. proposed a heating system based on the ASAHP aimed at improving the energy efficiency and decreasing the emission of pollution in the process of producing low-temperature hot water (Fig. 8) [103]. High-temperature hot water from the boiler (or the district heating network) was used to drive the AHP instead of being supplied to users directly, and the amount of heat could be increased because the evaporator is able to extract low-grade heat from the ambient air. The performances of the ASAHP using H_2O/LiBr and NH_3/$LiNO_3$ as the working fluids were simulated at different ambient temperatures. Next, the energy-saving potential was analyzed for the proposed system as applied in four typical Chinese cities. The results indicated that the ASAHP can provide energy conservation rates of 18%, 28.5%, 37% and 42% in Shenyang, Beijing, Shanghai and Guangzhou, respectively, demonstrating a great potential for future applications of low-temperature hot water.

Wu et al. [23] explored the suitable working pair and cycle configuration for heating and domestic hot water in cold regions; single-stage and double-stage ASAHP/GSAHP using NH_3–H_2O, NH_3–$LiNO_3$ and NH_3–NaSCN were also studied in this work. The results indicated that NH_3–$LiNO_3$ required a lower generation temperature and could operate at a lower evaporation temperature and higher condensation temperature than other solutions. In addition, the double-stage ASAHP/GSAHP is advantageous over the single-stage ASAHP/GSAHP in the use of a low-temperature driving source, the ability to operate in cold climates and the production of higher-temperature hot water. Finally, the applicability of different ASAHP/GSAHP cycles using different working pairs was analyzed in different cold regions. An Italian company developed a gas-fired ASAHP with a capacity of 38.4 kW (Fig. 9) that can produce hot water from 40 °C to 50 °C for building heating, and the heat pump performance has a low sensitivity to the outdoor air temperature [104].

Fig. 10 shows a schematic of the GSAHP. Compared with the ground source electrical heat pump (GSEHP), the system extracts less heat from and rejects more heat to the soil, which can reduce the ground thermal imbalance of heating-dominant areas. Therefore, the GSAHP may be a potentially useful system for heating and domestic hot water applications in cold regions [105].

For heating-dominant or heating-only buildings, the soil temperature around the ground heat exchanger will decrease gradually after continuous heat extraction in the heating season, which will consequently lead to performance degradation of the AHP. Wu et al. [106] proposed a hybrid system combining direct radiator cooling with a GSAHP using different working fluids. The average soil temperature and the outlet water temperature of the borehole were simulated dynamically. The results showed that the performance could be effectively improved by direct radiator cooling for all working pairs. The NH_3–$LiNO_3$ produced the best and most stable performance, whereas the COP of NH_3–H_2O and NH_3–NaSCN obviously decreased year by year with no cooling. The Italian company also developed a gas-fired GSAHP with a capacity of 42.6 kW (Fig. 11) and a nominal efficiency of 170% by means of heat recovery from a renewable source. This system can produce a 60% reduction in the borehole length compared with that of the GSEHP system.

5. Renewable and waste energy utilization

The use of renewable energy and the recovery of waste energy are unique strengths of the absorption refrigeration and heat pump systems because they can be directly driven by low-grade heat sources. The use of solar energy, geothermal energy, biomass energy and waste energy by the absorption cycles will be presented in the following sections.

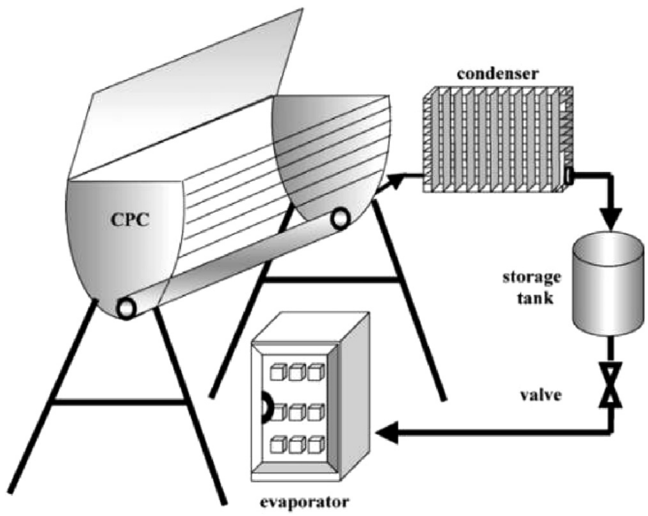


Fig. 12. Schematic of an intermittent solar absorption refrigeration system [41].

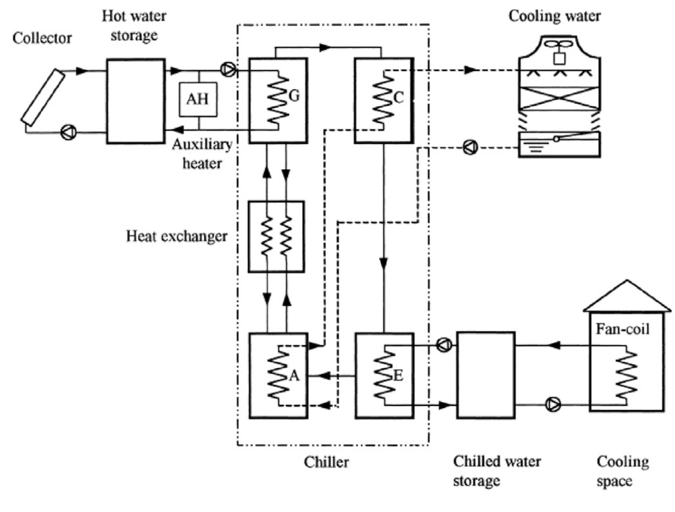


Fig. 13. Schematic of a continuous solar absorption refrigeration system [114].

5.1. Solar energy

The concept of solar cooling in buildings is appealing because it is one important contribution for the reduction of fossil fuel consumption and harmful emissions to the environment, and it is also quite attractive due to its low operating cost.

5.1.1. Basic absorption cycle

Certain analyses have been carried out to compare the differences between solar absorption cooling systems using H_2O–LiBr and those using NH_3–H_2O. Wilbur and Manchini [107] simulated a solar-powered absorption air-conditioning system consisting of conventional flat plate and evacuated tube collectors, a wet cooling tower and dry cooling towers and H_2O–LiBr and NH_3–H_2O as the working fluids for the application of hot water, chilled water or refrigerant storage. As a working fluid, H_2O–LiBr was shown to be superior to NH_3–H_2O. Ahmet Karakas et al. [108] presented an availability analysis for each component in the solar absorption cooling cycles using H_2O–LiBr and NH_3–H_2O and showed that the H_2O–LiBr system was more effective based on both first and second law analyses at temperatures above 0 °C. Nevertheless, the NH_3–H_2O mixture is still widely used due to the absence of crystallization and the low freezing point of the refrigerant.

(1) Intermittent absorption cycle

The intermittent absorption system can use solar energy in the daytime to provide cold production in the nighttime. Fig. 12 shows a schematic diagram of an intermittent solar absorption refrigeration system [41]. During the day, the mixture in the generator–absorber is heated by solar radiation, and subsequently, the ammonia is partially evaporated from the solution. The ammonia vapor is condensed in the condenser and stored in the refrigerant tank. During the night, the liquid ammonia passes through the expansion valve and produces the refrigeration effect in the evaporator.

Swartman and Swaminathan [109] successfully used solar energy to realize refrigeration in an intermittent system. Extensive tests had been carried out to determine the performance of NH_3–H_2O and NH_3–NaSCN solutions. The experimental results showed that the refrigerant–absorbent NH_3–NaSCN exhibited better performance than NH_3–H_2O. In addition, NH_3–NaSCN offers a lower equipment cost because it does not require a rectifying column to prevent the absorbent from being carried over to the condenser. Staicovici investigated [110] an intermittent single-stage NH_3–H_2O solar absorption system. Actual system COP values of 0.25–0.30 could be achieved at generation and condensation temperatures of 80 °C and 24.3 °C, respectively. For larger capacities of 450–675 MJ/day, the payback period was estimated at six and four years, respectively, over a lifetime of 15–18 years. El-Shaarawi et al. [111] designed an intermittently operated solar-powered NH_3–H_2O absorption system and presented a set of new polynomial forms of correlations, which were simple and easy to use to estimate the design parameters for both constant-pressure and constant-temperature absorption intermittent systems with a percentage error of less than 3%. Sierra [112] simulated a laboratory model of an NH_3–H_2O solar absorption refrigerator that operated intermittently. Tap water at 28 °C was used to remove the heat generated from the condensation. The COP for this unit operating under such conditions was in the range of 0.24–0.28. Hernández et al. [113] developed a direct and inverse artificial neural network approach to predict the required COP of a solar intermittent refrigeration system for ice production under various experimental conditions. With consideration of different solution concentrations, NH_3–$LiNO_3$ was used as a working fluid. The sensitivity analysis showed that the generation pressure was the most influential parameter for the COP, whereas the remaining input parameters were less significant.

(2) Continuous absorption cycle

Continuous solar absorption refrigeration systems are more widely used because they can provide lasting cooling and are therefore more advantageous over the intermittent absorption systems. Fig. 13 illustrates a typical schematic diagram of a continuous solar absorption refrigeration system [114].

Mansoori and Patel [115] conducted a quantitative comparative study of solar absorption cooling cycles using NH_3–H_2O, NH_3–NaSCN and H_2O–LiBr combinations and investigated the effect of the environmental temperatures and thermodynamic properties of the working fluids on the upper and lower limits for the COP. Shiran et al. [116] calculated various economic parameters from which the most favorable solar-operated NH_3–H_2O absorption refrigeration system may be selected. The results indicated the existence of various minimal operating parameters, e.g., collector outlet temperature. Uppal et al. [117] built a small-capacity solar-powered NH_3–H_2O absorption refrigerator to store vaccines in remote locations. Kouremenos et al. [118] simulated the performance of solar-driven NH_3–H_2O absorption units operating in conjunction with high- and intermediate-temperature solar collectors in Athens, and the theoretical COP, the maximum specific

cooling power, the heat gain factor and the heat gain power were predicted for the cases of refrigerators, heat pumps and heat transformers. Alvares and Trepp [119] performed a theoretical thermodynamic analysis on an NH_3–H_2O refrigeration cycle coupled to a solar water heating system using CPC collectors. Thirteen cycles were considered in the search for the maximum COP, and the exergetic performance was also investigated. Kouremenos [120] considered the addition of solar heat at the mean temperature level and the operation of a reversed absorption NH_3–H_2O cycle that split the solar heat into two components. One component is rejected at the evaporation side, and the other part is delivered for generation. The thermodynamics of the reversed cycle were examined, and its theoretical behavior was described. Hammad and Habali [121] designed a solar-powered absorption refrigeration cycle using an NH_3–H_2O solution to cool a vaccine cabinet in the Middle East. A year-round simulation indicated that the COP ranged between 0.5 and 0.65 with a generation temperature of 100–120 °C and an inside cabinet temperature of 0–8 °C. Francisco et al. [122] outlined the development and testing of a prototype of a 2-kW NH_3–H_2O absorption system designed for solar-powered refrigeration in small rural operations, in which all of the operations are manually controlled. The results suggested that future prototypes must be more compact and more efficient. Mendes et al. [123] tested a solar-assisted single-effect absorption machine using the NH_3–H_2O pair. The desorber featured a built-in adiabatic refining column composed of a rich solution spray. The refining method proved feasible, and the refining effect of the spray was nearly independent of the refrigerant vapor and solution mass flow rates. Abdulateef et al. [124] presented detailed thermodynamic design data and optimum design results for solar absorption refrigeration systems. The results showed that the NH_3–$LiNO_3$ and NH_3–NaSCN cycles yielded better performance than the NH_3–H_2O cycle, not only due to the higher COP values but also the lack of a need for analyzers and rectifiers. Abu-Ein [125] provided a detailed first law and second law analysis of a 10-kW solar absorption refrigeration system using NH_3–H_2O as a working medium. The minimum and maximum values of the COP and ECOP were observed at generation temperatures of 110 °C and 200 °C, respectively. Approximately 40% of the system exergy losses occurred in the generator. The maximum exergy losses in the absorber occurred at a generation temperature of 130 °C for all evaporation temperatures.

5.1.2. Advanced absorption cycle

The basic solar absorption cycle can be modified to achieve better performance, lower driving temperature, improved structure and other advantages.

Kaushik and Kumar [126] investigated NH_3–H_2O and NH_3–$LiNO_3$ pairs in an absorber heat recovery cycle in which the heat released during the absorption process is used to heat the strong solution exiting the absorber, thereby reducing the generator heat input and improving the COP. An improvement of approximately 10% was achieved in the COP, and the NH_3–$LiNO_3$ system yielded a higher COP than the NH_3–H_2O system over a wide range of conditions. The absorber heat recovery cycle is quite similar to that of the GAX cycle (Fig. 6); a schematic diagram of the former is shown in Fig. 14. The absorber is divided into two sections: the low-temperature section rejects heat to the ambient fluid, and the high-temperature section is used to preheat the incoming weak solution, thus reducing the heat input to the generator and consequently increasing the COP [127].

Arzoz et al. [93] reported the successful operation of a 3-kW double-stage NH_3–$LiNO_3$ absorption machine using low-temperature solar heat. A COP of 0.27 was obtained with a heat source temperature of 90 °C for an evaporation temperature of −15 °C and a condensation temperature of 45 °C. Ahachad et al. [128] studied a double-stage cascade absorption system (heat transformer and refrigeration machine) that successively employed H_2O–LiBr and NH_3–H_2O. The first-stage absorber produced heating water that circulated in the generator of the second stage. It was observed that the system can operate at lower hot source temperatures, and thus, it can be supplied either from flat plate collectors or from thermal effluents. Kouremenos et al. [129] studied a similar system. An optimization study for the individual and compound cycles was also carried out, and notably high performance was predicted. For example, the calculated theoretical COP was 219%, whereas the corresponding theoretical values for the single H_2O–LiBr and NH_3–H_2O units were 93% and 65%, respectively.

A diffusion absorption cycle uses a three-component working fluid consisting of the refrigerant (NH_3), the absorbent (H_2O or other absorbents) and the auxiliary gas (helium or hydrogen). The absorbent absorbs the refrigerant at low temperature and low partial pressure and releases it at high temperature against a high partial pressure. The auxiliary gas provides pressure equalization for the working fluid between the condenser and evaporator.

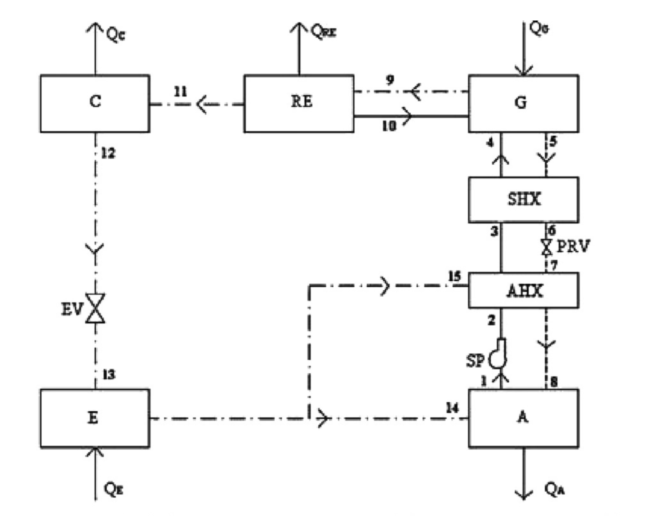


Fig. 14. Schematic of absorber heat recovery cycle.

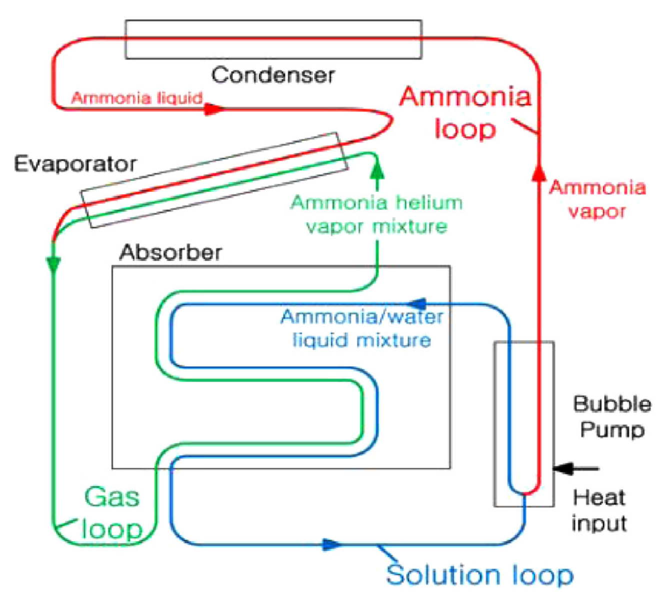


Fig. 15. Schematic of the diffusion absorption refrigeration cycle [130].

A schematic of the diffusion absorption refrigeration cycle is illustrated in Fig. 15 [130].

Jakob and Eicker [131] developed a solar power NH_3–H_2O diffusion absorption machine heated by CPC vacuum tube collectors with a capacity of 2.5 kW at temperatures between −10 °C and 5 °C. Helium was used to maintain the pressure equilibration between the high-pressure and low-pressure sides. The generator heating inlet temperatures ranged from 150 °C to 170 °C. In this case, the best observed cooling capacity was 1.5 kW, and the COP values observed were between 0.2 and 0.3. Wang [132] developed a new style of solar-driven diffusion–absorption refrigerator with solution pumps in which NH_3–$LiNO_3$–He was used as the working fluid, and an adiabatic spray absorber with a plate-type solution cooler was designed to enhance the mass and heat transfer, respectively. When the temperatures of generation, absorption and condensation were 87.0 °C, 29.6 °C and 21.6 °C, a typical operating experiment showed that the lowest evaporation temperature was–13.0 °C and the corresponding refrigeration capacity and COP were 1.9 kW and 0.156, respectively.

Absorption/compression systems have also been used for solar refrigeration due to their ability to make use of lower driving temperatures [133]. Ventaset al. [134] published an experimental study of a single-effect absorption chiller hybridized with an in-series low-pressure compression booster with an NH_3–$LiNO_3$ solution as the working fluid. The adiabatic absorber employed fog jet injectors, and the absorber pressures ranged between 429 and 945 kPa. For the same circulation ratio, the driving temperature decreased with a rise in the absorber pressure. The thermochemical compressor can produce a refrigerant with low driving temperatures, between 57 °C and 70 °C, which is interesting for solar cooling applications and low-temperature residual heat recovery.

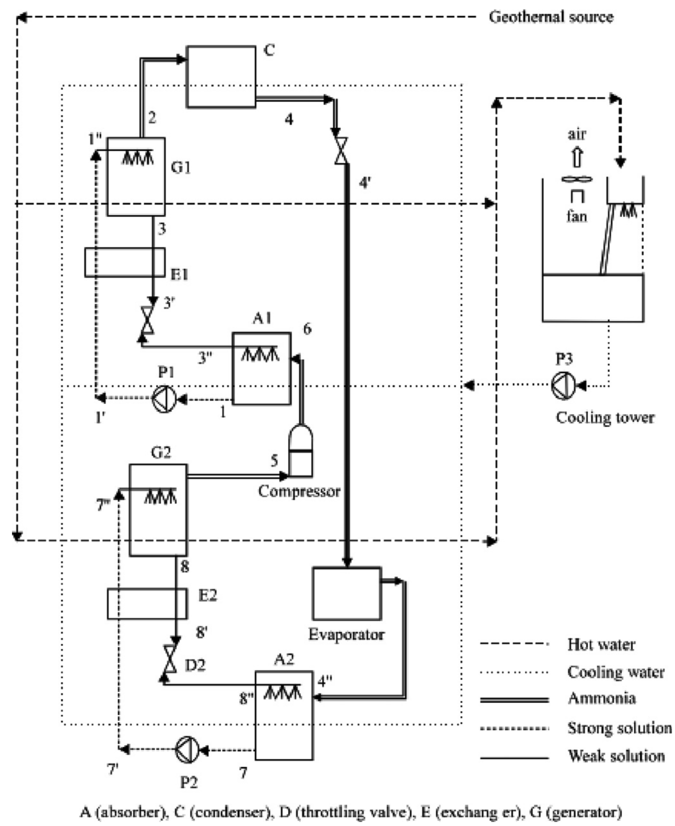


Fig. 16. Schematic of two-stage cycle with intermediate compression driven by geothermal energy [140].

5.2. Geothermal energy

In addition to solar energy, geothermal energy represents another type of widely applied renewable energy. Many research studies have been reported on the use of geothermal energy by a vapor-compression ground-source heat pump. The combination of geothermal energy and an absorption heat pump may offer a promising energy-efficient technology.

An attractive method for the use of low-enthalpy geothermal energy is the production of refrigeration using heat-driven absorption coolers. Best et al. [135] designed an NH_3–H_2O absorption cooler with a cooling capacity of 10.5 kW installed in a geothermal field. The unit operated successfully with generation temperatures as low as 91 °C and with cooling chamber temperatures as low as –5 °C. Later, this group carried out an experimental assessment of this system with ambient temperatures exceeding 40 °C and cooling water temperatures that reached 30 °C. The unit operated successfully with evaporative cooling loads that exceeded the design value [136]. Ayala et al. [137] modified this system for the use of NH_3–$LiNO_3$, and it was successfully operated at generation temperatures ranging from 90 °C to 145 °C and at cold chamber temperatures ranging from 0 °C to −10 °C.

Kairouani and Nehdi [138] presented the potential use and exploration of geothermal energy for cooling applications in a combined cascade system that used R134a for the compression portion and NH_3–H_2O for the absorption portion. The geothermal source temperature was in the range of 70–76 °C, the condensation temperature was 35 °C and the R134a evaporation temperature was −10 °C for ice production, with a COP of approximately 5.4. Based on the typical geothermal energy sources of Tunisia, which demonstrated a potential refrigeration power of 9.1 MW, the quantity of ice that could be produced was nearly 82 t per hour. The CO_2 emissions should thus be reduced by approximately 5884 t per year (a reduction of 59%). Subsequently, three refrigerants (R717, R22 and R134a) were studied for the compression portion of the described cascade system. The results showed that the COP of the cascade system could be improved by 37–54% compared with the conventional cycle [139]. This group also analyzed a double-stage cycle based on the NH_3–H_2O absorption system with intermediate compression, which raised the pressure of the ammonia vapor emitted from the low-pressure generator to supply the high-pressure absorber as shown in Fig. 16. The two generators of the system were heated by geothermal energy at low temperature. Based on the electric consumption for T_g=62 °C, T_c=T_a=35 °C and T_e=−10 °C, the system efficiency was 8.2 [140].

5.3. Biomass energy

Biomass is another potential alternative renewable energy source, especially in rural areas where large amounts of biomass can be used as the energy source for absorption systems. Until recently, research on the utilization of biomass has been limited. Siddiqui [141] conducted an optimization study of the generation temperatures in NH_3–H_2O, NH_3–$LiNO_3$, NH_3–NaSCN and H_2O–LiBr absorption cycles to achieve a minimum cost for the energy source. A comparative study among the costs of the energies (biogas, liquefied petroleum gas and solar collectors) in the various cycles has been carried out. Empirical equations for the identification of the heating values and the costs of the energy sources have been presented. Villela and Silveira [142] proposed the use of biogas generated in the wastewater treatment plants of the dairy industry. A thermoeconomic analysis was applied to the supplementary cold water production of an NH_3–H_2O absorption refrigeration system driven by the burning of biogas. It was concluded that the absorption refrigeration system was superior to the compression refrigeration system if the biogas cost was not considered. Huang et al. [143] simulated a commercial building

Table 4
Summary of renewable energy utilization and waste heat recovery by ammonia-based absorption systems.

Renewable energy/waste heat	Cycle	Working fluid	Typical application	Remark
Solar energy	Intermittent single-stage	NH_3–H_2O [109–112]	Refrigerator	System COP=0.25–0.30 (T_g=80 °C, T_c=24.3 °C)
	Intermittent single-stage	NH_3–NaSCN [109]	Refrigeration	NH_3–NaSCN has higher COP and lower costs than NH_3–H_2O
	Intermittent single-stage	NH_3–$LiNO_3$[41,83,113]	Ice production	Generation pressure is the most influential parameter on COP
	Intermittent single-stage	NH_3–$LiNO_3$–H_2O[83]	Ice production	NH_3–$LiNO_3$–H_2O can be 24% higher than NH_3–$LiNO_3$ in COP
	Continuous single-stage	NH_3–H_2O [115–123]	Vaccines storage, refrigerator	COP=0.5–0.65 (T_g=100–120 °C, cabinet inside temperature=0–8 °C)
	Continuous single-stage	NH_3–NaSCN[115,124]	Cooling, refrigeration	NH_3–NaSCN was better than NH_3–H_2O
	Continuous single-stage	NH_3–$LiNO_3$ [124]	Refrigeration	NH_3–$LiNO_3$ was better than NH_3–H_2O
	Absorber heat recovery	NH_3–H_2O, NH_3–$LiNO_3$[126]	Refrigeration	COP improvement was approximately 10%
	Double-stage	NH_3–LiNO3[93]	Refrigeration	COP=0.27 (T_g=−90 °C, T_e=−15 °C and T_c=−45 °C)
	Double-stage cascade	H_2O–LiBr+NH_3–H_2O [128,129]	Heat transformer, refrigeration	The system can be operated at lower hot source temperatures
	Diffusion absorption	NH_3–H_2O–He [131] NH_3–$LiNO_3$–He [132]	Cooling, refrigerator	COP=0.2–0.3 (generator inlet temperature: 150–170 °C)
	Absorption/compression	NH_3–$LiNO_3$ [124]	Cooling	Very low driving temperatures (57–70 °C)
Geothermal energy	Single-stage	NH_3–H_2O [135,136] NH_3–$LiNO_3$[137]	Cooler	Installed at the geothermal field; cold chamber=0–−10 °C; T_g=90–145 °C
	Double-stage cascade	R134a+NH_3–H_2O [138]; R717/R22/R134a+NH_3–H_2O [139]	Ice production	Geothermal source: 70–73 °C; T_c=35 °C; T_e=−10 °C
	Double-stage +compression	NH_3–H_2O [140]	Ice production	T_g=62 °C, T_c=T_a=35 °C, T_e=−10 °C
Biomass energy	Single-stage	NH_3–H_2O, NH_3–$LiNO_3$, NH_3–NaSCN [141]	Refrigeration	Biogas, liquefied petroleum gas and solar collectors were studied
	Single-stage	NH_3–H_2O [142]	Cold water production	Biogas was generated in the wastewater treatment plant
	Single-stage	NH_3–H_2O [142]	Commercial building scale tri-generation	Willow, rice husk and miscanthus were studied
Waste heat recovery	Single-stage	NH_3–H_2O [144]	Fishing vessel	Heat was recovered from engine exhausts
	Single-stage	NH_3–H_2O [145]	Refinery	Provide refrigeration for two process streams while being powered by waste heat from a third process stream
	Single-stage	NH_3–H_2O [146,147]	Heat recovery in LNG plant	Recovering waste heat from a 9 MW electricity generation process could save 1.9 MW of electricity consumption
	GAX	NH_3–H_2O [148]	Waste heat utilization	Parametric analysis was performed to study the effects of the waste heat source temperature on the performance

scale tri-generation plant fueled by a biomass downdraft gasifier with an ammonia absorption system used to supply the cooling. The study also examined the impact of different biomass feedstock (willow, rice husk and miscanthus) on the performance of a tri-generation plant.

5.4. Waste heat recovery

Fernández-Searaet al. [144] presented a parametric analysis of a gas-to-thermal fluid heat recovery system from engine exhausts in a fishing vessel used to power an NH_3–H_2O absorption refrigeration plant for onboard cooling production. The major components of the system are fluid-to-solution and gas-to-fluid heat exchangers. Both heat exchangers and the complete system were modeled to study the influence of the geometric design parameters and thermal operating conditions on the heat exchangers and system thermal performance. The optimal design based on real data was tested, and the operating function of the exhaust gas bypass control was obtained. Erickson et al. [145] studied a waste-heat-powered NH_3–H_2O absorption refrigeration system installed at the Ultramar Diamond Shamrock refinery to recover propane and higher-molecular-weight hydrocarbons. The system was designed to provide refrigeration for two process streams at the refinery using power from waste heat via a third process stream. The refrigeration benefited the refinery by recovering salable product and increasing the capacity of the process units with no additional electrical demand. Kalinowski et al. [146] proposed use of an absorption refrigeration system powered by waste heat from an electrical-power-generation gas turbine to provide low-temperature cooling for the recovery process of liquefied natural gas (LNG). The analysis showed that the recovery of waste heat from a 9-MW electrical generation process could save 1.9 MW of electricity consumption by producing additional cooling to the LNG plant. Application of the integrated cooling, heating and power represented an excellent energy conservation option for the oil and gas industry. Somers detailed the modeling procedure for single-effect NH_3–H_2O chillers used to recover LNG plant waste heat to provide cooling and improve energy efficiency, which is especially valuable in the oil and gas industry. Each model was integrated with a gas turbine as a waste heat source, and parametric studies were conducted for a range of partial load conditions, evaporation temperatures and ambient conditions. Finally, the best chiller design was selected, and an annual performance study was conducted to quantify the expected cooling

performance and related energy savings [147]. Kang et al. [148] developed an advanced GAX to reduce the generator exit temperature to the highest extent possible using waste heat sources. Additional parametric analysis was performed to study the effects of the waste heat source temperature on the cycle performance.

The use of renewable energy and waste heat recovery in different absorption cycles with various ammonia-based working fluids are summarized in Table 4. It can be observed that solar energy is quite popular, whereas the applications and research studies regarding geothermal and biomass energy are relatively fewer in number. For waste heat recovery, the working fluid is mainly NH_3–H_2O, with a few studies conducted on other ammonia-based solutions.

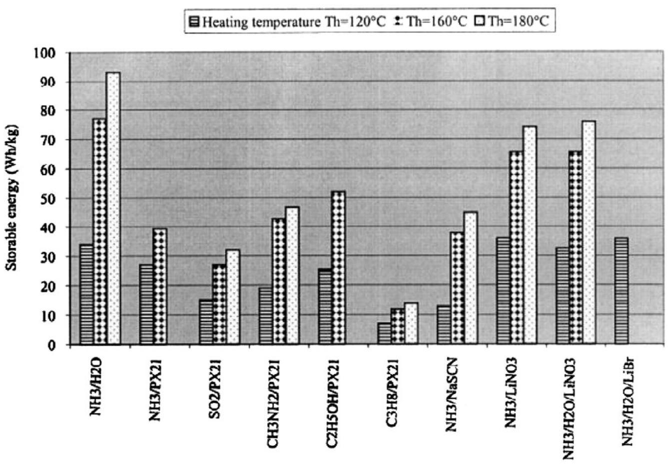


Fig. 17. Storage capacity of absorption and adsorption for an evaporation temperature of −20 °C, an ambient temperature of 35 °C and three different heating temperatures (120 °C, 160 °C and 180 °C) [151].

Table 5
Storage capacity of different absorption working fluids for solar cooling and refrigeration.

Application	Working fluid	Storage capacity (Wh/kg)
Solar refrigeration	NH_3–H_2O	34
$T_e=-20$ °C, $T_g=120$ °C, $T_a=35$ °C	NH_3–$LiNO_3$	36
Solar cooling	NH_3–H_2O	110
$T_e=5$ °C, $T_g=120$ °C, $T_a=35$ °C	NH_3–$LiNO_3$	89
	H_2O–NaOH	277
	CH_3OH–LiBr	133
	H_2O–CH_3NH_2	77

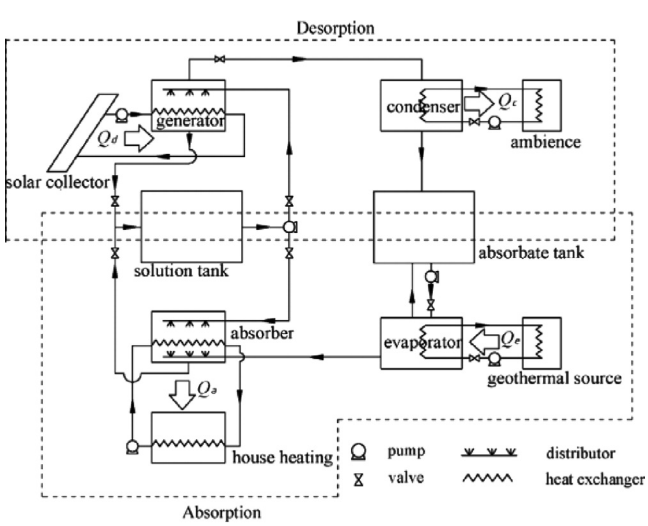


Fig. 18. Schematic of a seasonal absorption energy storage system for house heating [152].

6. Thermal energy storage

Thermal energy storage plays an important role in matching energy supply with energy demand, which is especially significant in low-grade energy uses, such as solar energy and waste heat. Absorption systems can realize thermal energy storage and offer many advantages [149]:

- The storage temperature is close to the ambient temperature, and the systems are suitable for long-term thermal energy storage;
- the driving energy source is variable, including solar energy, industrial waste heat and electricity, among others;
- the types of energy supply can be diverse, and the latent energy stored in the solution can be converted to meet the demands for cooling, heating and dehumidification;
- the high energy release rate allows the system to rapidly accommodate desired requirements;
- the systems are environmentally friendly, with low ozone depletion and limited global warming potential.

Rizza [150] considered the analysis of a low-temperature NH_3–H_2O thermal storage system designed to shift the electricity demand from high- to low-demand periods. The stored thermal capacity was usable at a temperature of −27 °C and above. The generator heat was supplied by a self-contained vapor compression heat pump operated during the off-peak period to recover the low-temperature thermal storage. The ammonia vapor liberated from the rectifier was used in the compressor to produce the generator heat. Three different configurations were considered, including a solar-assisted system. The results were compared with those from a eutectic salt storage system.

Mugnier and Goetz [151] compared the storage capacity given in mass units or volume units of a sorbent for different sorption systems for cooling and refrigeration. The energy storage capacities per kilogram of a rich composition of different absorption and adsorption working pairs under different heating temperatures are shown in Fig. 17. Additionally, the storage capacity values of different absorption working fluids for solar cooling and refrigeration are listed in Table 5. It can be concluded that ammonia-based working fluids are not the best choice in terms of energy storage capacity and cycle efficiency, but they prevail in subfreezing refrigeration applications rather than the typical air-conditioning applications.

Liu et al. [152] presented a seasonal energy storage system for house heating (Fig. 18). The solar energy was stored during the summer via desorption, and the heat was released during the winter through absorption, with low-temperature geothermal heat extracted by the evaporator. The storage capacity and efficiency of seven absorption couples (i.e., H_2O–$CaCl_2$, H_2O–glycerin, H_2O–KOH, H_2O–LiBr, H_2O–LiCl, H_2O–NaOH and NH_3–H_2O) were also studied. The storage capacity and efficiency of NH_3–H_2O versus the temperature of absorption is shown in Fig. 19. Comparisons of different absorption couples indicated that the storage capacity and price of NH_3–H_2O were acceptable, but this system was disadvantaged by the temperature requirement of the solar energy (> 150 °C) and by security issues.

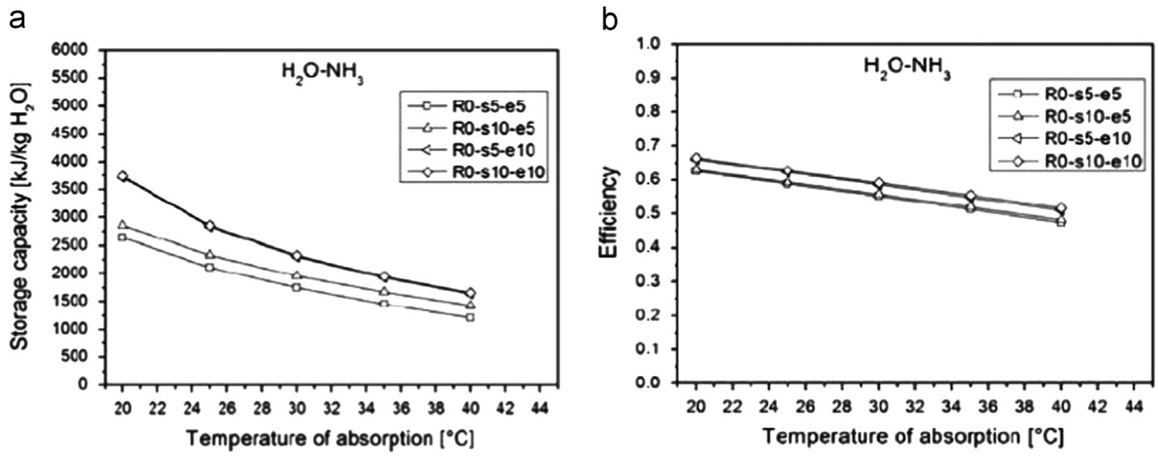


Fig. 19. The storage capacity and efficiency of NH_3–H_2O versus the temperature of absorption [152].

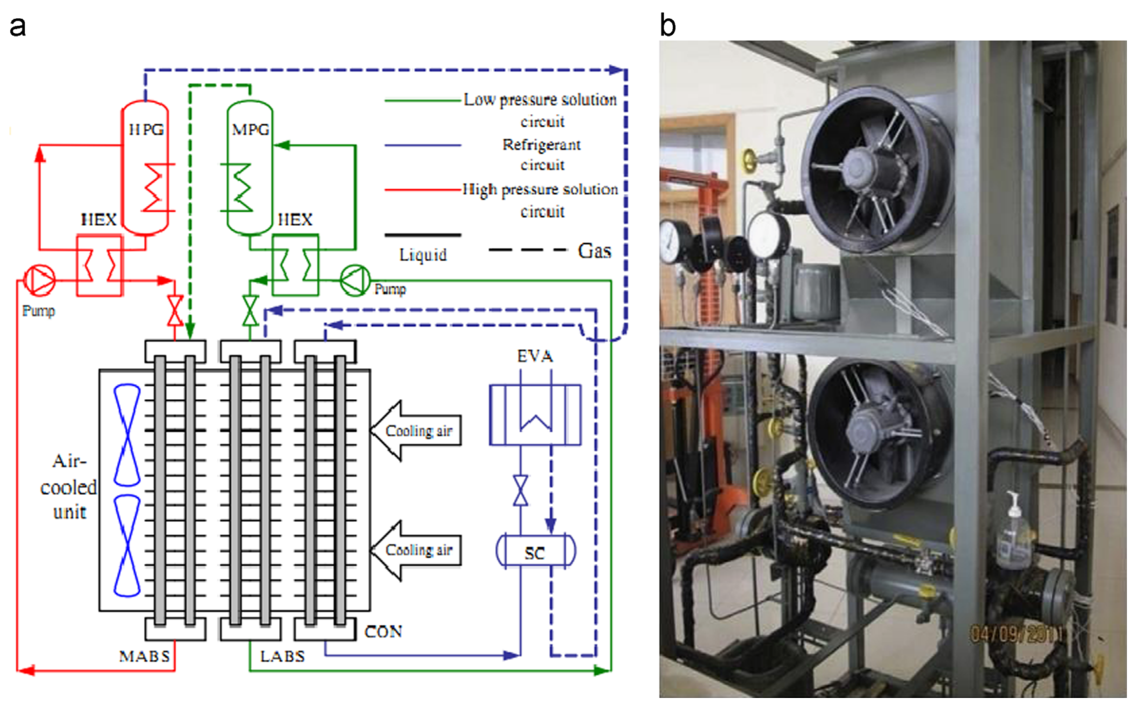


Fig. 20. Air-cooled two-stage NH_3–H_2O absorption refrigeration system. (a) Schematic diagram [157], (b) experimental prototype [158].

7. Miniaturization of absorption systems

Miniaturization of absorption systems is essential for residential applications. Air-cooled absorption, which eliminates the cooling water system, and diffusion absorption, which removes the solution pump, are two important cycles for the purpose of miniaturization [153].

Oronel et al. [154] carried out an experimental study of air-cooled absorption systems driven by low-temperature heat sources using NH_3–$LiNO_3$ and NH_3–$LiNO_3$–H_2O mixtures. The mass absorption flux and the solution heat transfer coefficient achieved with the ternary mixture were approximately 1.3–1.6 and 1.4 times higher, respectively, than those of the binary mixture under similar operating conditions, mainly due to the lower viscosity of the ternary mixture and the high affinity of ammonia for water. Empirical correlations for the solution Nusselt and Sherwood numbers were also reported.

Velázquez and Best [155] presented a numerical analysis and energy evaluation of an air-cooled NH_3–H_2O GAX absorption system operated with a hybrid natural gas–solar energy source, which was expected as an alternative for space conditioning in the residential sector. The unit was designed with a cooling capacity of 10.6 kW, and a COP of 0.86 was calculated.

Francisco et al. [156] constructed a prototype of an NH_3–H_2O absorption chiller with a 2-kW cooling capacity. The condenser and the absorber were air-cooled by natural convection, and the solution pump was replaced with a transfer tank. The work was meaningful although the experimental COP was lower than 0.05.

Lin et al. [157] simulated an air-cooled two-stage NH_3–H_2O absorption refrigeration system driven by 85 °C hot water supplied from a solar collector and showed that the thermal COP was 0.34 and the electrical COP was 26 under typical summer conditions. Circular-finned tube bundles were selected to build the air-cooled equipment. The condenser was arranged in front of the absorber to obtain an optimum system performance. The low-pressure absorber was arranged in front of the middle pressure absorber to minimize the absorption length. This configuration of the air-cooled equipment is suggested for a 5-kW cooling capacity system

(Fig. 20(a)). Du et al. [158] built an experimental prototype for this air-cooled two-stage NH_3–H_2O absorption refrigeration system with a 2-kW cooling capacity to investigate the feasibility and performance of the proposed system (Fig. 20(b)). When the prototype was driven by 85 °C hot water with an evaporation temperature of 8 °C and an ambient air temperature of 29 °C, its thermal COP and electric efficiency reached 0.21 and 5.1, respectively. The COP stabilized in the range of 0.18–0.25, and the electric efficiency varied between 3.6 and 5.1. This system provided a method for the development of low-cost small bulk solar absorption air-conditioning systems for residential applications.

Jakob and Pink [159] reported on a 10-kW single-effect NH_3–H_2O absorption chiller with a membrane pump for residential and commercial applications that was developed by a company in Germany. The COP reached 0.64 for a cooled ceiling air-conditioning system when the driving temperatures were 75–68 °C, the cooling water temperatures were 24–29 °C and the chilled water temperatures were 19–16 °C. Häberle et al. [160] described an air-cooled NH_3–H_2O absorption chiller with a cooling capacity of 17 kW produced by a company in Italy. The chiller was driven by pressurized water from a Fresnel collector, and the driving temperatures required were 180–200 °C.

Diffusion absorption is also a satisfactory solution for the miniaturization of absorption systems. Wang [161] developed a new style of diffusion absorption refrigeration system driven by heat sources with low temperatures. The NH_3–$LiNO_3$–He was used as a working fluid, and a spray absorber with a solution cooler was designed to enhance the mass and heat transfer. The experiments showed that the system was able to meet the temperature requirements for air conditioning when the heat source temperature was between 70 °C and 83 °C. The refrigeration capacity and the COP varied in the range of 1.90–4.22 kW and 0.177–0.332, respectively. Abdullah and Hieng [162] evaluated the transient temperature performance of an NH_3–H_2O–H_2 diffusion absorption cooling system′s components for two types of energy sources (electric energy and liquid petroleum gas), and an economic study was carried out for three different energy sources (electric, liquid petroleum gas and solar energy). Liu et al. [163] presented selected parameters that affected the performance of a NH_3–NaSCN diffusion absorption refrigeration system. By comparing the simulation and experimental data, this group showed that the COP of the NH_3–NaSCN diffusion absorption device with a 2-kW cooling capacity could reach 0.4 when the regeneration temperature was 80° to 105 °C, the concentration was 0.38–0.5 and the condensation temperature was 30 °C.

8. Conclusions and suggestions

Ammonia-based absorption working fluids have unique advantages over H_2O–LiBr fluids due to a low freezing temperature, zero risk of crystallization and no need for vacuum maintenance. These characteristics make ammonia-based absorption chillers and heat pumps irreplaceable in a wide range of applications. This paper comprehensively reviews the ammonia-based absorption chillers and heat pumps, including the thermodynamic and physical properties of different ammonia-based working fluids; developments and applications in low-temperature refrigeration, heating and DHW; renewable energy utilization; waste heat recovery; thermal energy storage; and the miniaturization of AHPs.

For binary ammonia-based working fluids, NH_3–NaSCN and NH_3–$LiNO_3$ have been widely studied to eliminate the rectifier in NH_3–H_2O absorption systems. Additionally, NH_3–NaSCN and NH_3–$LiNO_3$ have been proven to require lower driving temperatures and can achieve higher energy performances than the conventional NH_3–H_2O systems, which allows for the use of lower temperature heat sources, including solar energy, geothermal energy and waste heat. However, the performance may be limited by the high viscosity of the salt solutions. To solve this problem, ternary ammonia-based working fluids (i.e., NH_3–H_2O–LiBr, NH_3–H_2O–$LiNO_3$ and NH_3–H_2O–hydroxide) were proposed to lower the solution viscosity and improve the heat transfer coefficient. It should be noted that the boiling temperatures of NH_3–H_2O–LiBr and NH_3–H_2O–$LiNO_3$ are higher than those of binary mixtures, and thus, a higher driving temperature is required. In contrast, for NH_3–H_2O–hydroxide, a lower driving temperature than that required for NH_3–H_2O cycles can meet the demand. However, the hydroxide in the ternary mixture will tend to salt out the ammonia from the absorber and lead to poor absorption.

The thermodynamic and physical properties of pure ammonia and binary and ternary ammonia mixtures are presented in this work. The properties of ternary working fluids require further research to guide the evaluation, design and simulation of such absorption systems.

Ammonia-based absorption chillers can operate at temperatures well below normal air-conditioning temperatures, which may be useful for subzero refrigeration applications. For operation at lower refrigeration temperatures, advanced absorption cycles such as the double-stage cascade cycle, double-stage absorption and hybrid absorption/compression cycle can be applied. The evaporation temperatures for single-stage absorption systems lie mainly in the range of −30 °C to −5 °C, whereas advanced absorption chillers can reach evaporation temperatures as low as −70 °C.

The lack of crystallization and the low freezing point of NH_3 make ammonia-based solutions promising technologies for heating and DHW applications. Absorption systems operating in heat pump mode have become competitive with the most widely used vapor compression heat pumps in terms of environmental impact as well as energy efficiency. It is recommended that the ASAHP and GSAHP systems be employed for heating and DHW applications, especially in cold regions, where the ASEHP performs badly or fails to operate in notably cold climates due to the high compression ratio and the GSEHP suffers from performance deterioration caused by thermal imbalance. The GSAHP can reduce the ground thermal imbalance of heating-dominant systems and requires fewer boreholes than the GSEHP in heating-only systems.

Ammonia-based absorption systems using various working fluids driven by solar energy are quite popular, whereas the applications of and research on geothermal and biomass energy are relatively scarce. For waste heat recovery, the working fluid is mainly NH_3–H_2O, though a few studies of other ammonia-based solutions have been published as well.

Comparisons of different absorption thermal storage cycles have indicated that ammonia-based working fluids are not the best choice for energy storage capacity and cycle efficiency, but they prevail in subfreezing refrigeration rather than the typical air-conditioning applications.

Air-cooled absorption and diffusion absorption are two important approaches used to realize the miniaturization of absorption systems, which is essential for residential applications. Ammonia-based working fluids are also attractive due to the absence of crystallization, which is a persistent problem for H_2O–LiBr systems that is caused by poor cooling conditions.

Acknowledgment

The authors gratefully acknowledge the support from the Natural Science Foundation for Distinguished Young Scholars of China (Grant no. 51125030) and the National Basic Research Program of China (Grant no. 2010CB227305).

Appendix A. Properties of pure NH_3

Appendix A.1. Sun model [39]

VLE	$P(T)=10^3\sum_{i=0}^{6}a_i(T-273.15)^i$	(A1)
Liquid enthalpy	$h_l(T)=\sum_{i=0}^{6}b_i(T-273.15)^i$	(A2)
Vapor enthalpy	$h_v(T)=\sum_{i=0}^{6}c_i(T-273.15)^i$	(A3)

Coefficients of Eqs. (A1)–(A3)

i	a_i	b_i	c_i
0	4.2871e−1	1.9879e2	1.4633e3
1	1.6001e−2	4.4644e0	1.2839e0
2	2.3652e−4	6.2790e−3	−1.1501e−2
3	1.6132e−6	1.4591e−4	−2.1523e−4
4	2.4303e−9	−1.5262e−6	1.9055e−6
5	−1.2494e−11	−1.8069e−8	2.5608e−8
6	1.2741e−13	1.9054e−10	−2.5964e−10
Standard error	1.6e−3	8.5626e0	1.059e1
Mean deviation	1.252e−2	5.566e−3	3.679e−3

Appendix A.2. Cleland model [59]

VLE	$p_{sat}=\exp\left(a_1+\frac{a_2}{T_{sat}+a_3}\right);\ T_{sat}=\frac{a_2}{\ln p_{sat}-a_1}-a_3$	(A4)
Liquid enthalpy	$h_l=a_4+a_5T_1+a_6{T_1}^2+a_7{T_1}^3$	(A5)
Saturated vapor enthalpy	$h_{i1}=a_8+a_9T_{sat}+a_{10}T_{sat}^2+a_{11}T_{sat}^3;\ h_v=h_{i1}+a_{12}$	(A6)
Superheated vapor enthalpy	$\frac{h_{i2}}{h_{i1}}=1+a_{13}\Delta T_{SH}+a_{14}\Delta T_{SH}^2+a_{15}(\Delta T_{SH})(T_{sat})+a_{16}(\Delta T_{SH})^3(T_{sat})$ $+a_{17}(\Delta T_{SH})(T_{sat})^2+a_{18}(\Delta T_{SH})^2(T_{sat})^2$ $h_s=h_{i2}+a_{12}$	(A7)
Specific volume of saturated vapor	$v_s=(a_{21}+a_{22}T_{sat}+a_{23}T_{sat}^2+a_{24}T_{sat}^3)\exp\left(a_{19}+\frac{a_{20}}{T_{sat}+273.15}\right)$	(A8)
Specific volume of superheated vapor	$\frac{v}{v_s}=1+a_{25}\Delta T_{SH}+a_{26}\Delta T_{SH}^2+a_{27}(\Delta T_{SH})(T_{sat})$ $+a_{28}(\Delta T_{SH})^2(T_{sat})+a_{29}(\Delta T_{SH})(T_{sat})^2+a_{30}(\Delta T_{SH})^2(T_{sat})^2$	(A9)

Coefficients of Eqs. (A4)–(A9)

a_1	a_2	a_3				e/%
22.11874	−2233.8226	244.20				0.08
a_4(IIR)	a_4(ASHRAE)	a_5	a_6	$a_7\times10^{-3}$		e/(kJ/kg)
200,000	184,311	4751.63	2.0449	−37.875		0.27
a_8	a_9	a_{10}	$a_{11}\times10^{-3}$	a_{12}(IIR)	a_{12}(ASHRAE)	e/(kJ/kg)
1,441,467	920.154	−10.20556	−26.5126	15,689	0	0.10
$a_{13}\times10^{-3}$	$a_{14}\times10^{-3}$	$a_{15}\times10^{-3}$	$a_{16}\times10^{-3}$	$a_{17}\times10^{-3}$	$a_{18}\times10^{-3}$	e/%
1.68937	−3.47675	7.55525	−3.04755	9.79201	−3.62549	0.27
a_{19}	a_{20}	a_{21}	$a_{22}\times10^{-3}$	$a_{23}\times10^{-3}$	$a_{24}\times10^{-3}$	e/%
−11.09867	2691.680	0.99675	4.02288	2.64170	−1.75152	0.16
$a_{25}\times10^{-3}$	$a_{26}\times10^{-3}$	$a_{27}\times10^{-3}$	$a_{28}\times10^{-3}$	$a_{29}\times10^{-3}$	$a_{30}\times10^{-3}$	e/%
4.77321	−3.11142	1.58632	−0.91676	2.97255	−0.86668	0.53

*e means the maximum deviation between Cleland and Chan [164].

Appendix B. Properties of NH_3–H_2O

Appendix B.1. Schulz model [62]

The equations of state of NH_3–H_2O solution are expressed as follows:

For pure component

Gas phase

$$G_R^g = H_0^g - \theta S_0^g + \int_{\theta_0}^{\theta} C_{PR}^{ig} d\theta - \theta \int_{\theta_0}^{\theta} \frac{C_{PR}^{ig}}{\theta} d\theta + \theta \ln \frac{\pi}{\pi_0} + C_1\theta(\pi - \pi_0) + C_2(\pi - \pi_0) + C_3\left(\frac{\pi}{\theta} + \theta\frac{\pi_0}{\theta_0^2} - 2\frac{\pi_0}{\theta_0}\right) \quad \text{where } C_{PR}^{ig} = D_1 + D_2\theta + D_3\theta^2 \qquad \text{(B1)}$$

Liquid phase

$$G_R^g = H_0^f - \theta S_0^f + \int_{\theta_0}^{\theta} C_{PR}^{if} d\theta - \theta \int_{\theta_0}^{\theta} \frac{C_{PR}^{if}}{\theta} d\theta + A_1(\pi - \pi_0) + A_2\left(\frac{\pi^2 - \pi_0^2}{2}\right) + A_3\theta(\pi - \pi_0) + A_4\theta^2(\pi - \pi_0) \quad \text{where } C_P^i R^f = B_1 + B_2\theta \qquad \text{(B2)}$$

For mixture

Gas phase

$$G_R^{g^M} = (1-y)G_R^{g^{H_2O}} + yG_R^{g^{NH_3}} + \theta(1-y)\ln(1-y) + \theta y \ln y \qquad \text{(B3)}$$

Liquid phase

$$G_R^{f^M} = (1-x)G_R^{f^{H_2O}} + xG_R^{f^{NH_3}} + \theta(1-x)\ln(1-x) + \theta x \ln x + G_R^e \quad \text{where } G_R^e = \{F_1 + F_2\pi + F_3\pi^2 + (F_4 + F_5\pi)/\theta + (F_6 + F_7\pi)/\theta^2 + F_8/\theta^3 + [F_9 + F_{10}\pi + F_{11}\pi^2 + (F_{12} + F_{13}\pi)/\theta](2x-1) + (F_{14} + F_{15}\pi + F_{16}/\theta)(2x-1)^2\}x(1-x) \qquad \text{(B4)}$$

Parameter specification

$\theta = \frac{T}{T_b} \pi = \frac{P}{P_b} G_R = \frac{G_m}{R_m T_b} C_{PR} = \frac{C_{Pm}}{R_m}$

T_b=100 K; P_b=1 MPa; R_m=8.3143 J/(mol K)

g (gas phase); *f*(liquid phase); *M*(mixture); *e*(excessive); *i*(component label)

R(relative value); *b*(base value); *m*(molar parameters)

x, *y* is the molar fraction of NH_3 in liquid and vapor mixture, respectively.

From the above equations of state, the required thermodynamic properties of the working fluid can be derived as follows:

Vapor–liquid equilibrium of pure NH_3

$$G_R^{f^{NH_3}} - G_R^{g^{NH_3}} = 0 \qquad \text{(B5)}$$

Vapor–liquid equilibrium of NH_3–H_2O

TPX relations

$$f(T,P,x) = \exp\left\{\frac{1}{\theta}\left[G_R^{f^{H_2O}} + \theta\ln(1-x) + G_R^e - x\left(\frac{\partial G_R^e}{\partial x}\right)_{\theta,\pi} - G_R^{f^{H_2O}}\right]\right\} + \exp\left\{\frac{1}{\theta}\left[G_R^{f^{NH_3}} + \theta\ln x + G_R^e + (1-x)\left(\frac{\partial G_R^e}{\partial x}\right)_{\theta,\pi} - G_R^{g^{NH_3}}\right]\right\} - 1 = 0 \qquad \text{(B6)}$$

TPY relations

$$f(T,P,y) = \exp\left\{\frac{1}{\theta}\left[G_R^{f^{NH_3}} + \theta\ln x + G_R^e + (1-x)\left(\frac{\partial G_R^e}{\partial x}\right)_{\theta,\pi} - G_R^{g^{NH_3}}\right]\right\} - y = 0 \qquad \text{(B7)}$$

Vapor enthalpy of NH_3–H_2O

$$H_R^{g^M} = (1-y)\left[G_R^g H_2O - \theta\left(\frac{\partial G_R^{g^{H_2O}}}{\partial \theta}\right)_\pi\right] + y\left[G_R^{g^{NH_3}} - \theta\left(\frac{\partial G_R^{g^{NH_3}}}{\partial \theta}\right)_\pi\right] \qquad \text{(B8)}$$

Liquid enthalpy of NH_3–H_2O

$$H_R^{f^M} = (1-x)\left[G_R^{f^{H_2O}} - \theta\left(\frac{\partial G_R^{fg^{H_2O}}}{\partial \theta}\right)_\pi\right] + x\left[G_R^{f^{NH_3}} - \theta\left(\frac{\partial G_R^{f^{NH_3}}}{\partial \theta}\right)_\pi\right] + G_R^e - \theta\left(\frac{\partial G_R^e}{\partial \theta}\right)_{\pi,x} \qquad \text{(B9)}$$

Coefficients of Schulz equations

	Pure component		Mixture	
	H_2O	NH_3		
A_1	0.026949	0.0318219	F_1	25.5078
A_2	−0.000009958	−0.000050416	F_2	0.4935
A_3	−0.0040529	−0.0071294	F_3	−0.0115994

A_4	0.00077344	0.0026517	F_4	−165.353
B_1	7.7221	6.18881	F_5	−2.57531
B_2	0.393864	1.26706	F_6	256.593
C_1	−0.176416	−0.203312	F_7	3.25854
C_2	2.30417	1.83950	F_8	−149.857
C_3	−8.28598	−4.69069	F_9	1.60532
D_1	4.09249	3.82918	F_{10}	0.284681
D_2	−0.089058	0.02369	F_{11}	−0.0053865
D_3	0.023875	0.04495	F_{12}	−0.784
θ_0	5.0699	3.2515	F_{13}	−0.775995
π_0	3.00	2.141	F_{14}	0.37872
H_0^g	60.9347	26.6392	F_{15}	0.0225936
H_0^f	21.7697	5.20916	F_{16}	8.00572
S_0^g	13.4420	8.29281		
S_0^f	5.71697	1.70201		

Appendix B.2. ***Patek model*** [66]

Vapor–liquid equilibrium

$$T(p,x)=T_0\sum_i a_i(1-x)^{m_i}\left[\ln\left(\frac{p_0}{p}\right)\right]^{n_i}\quad T_0=100\text{ K},\ p_0=2\text{ MPa} \tag{B10}$$

$$T(p,y)=T_0\sum_i a_i(1-y)^{m_i/4}\left[\ln\left(\frac{p_0}{p}\right)\right]^{n_i}\quad T_0=100\text{ K},\ p_0=2\text{ MPa} \tag{B11}$$

$$y(p,x)=1-\exp\left[\ln(1-x)\sum_i a_i\left(\frac{p_0}{p}\right)^{m_i}x^{n_i/3}\right]\quad p_0=2\text{ MPa} \tag{B12}$$

Liquid enthalpy

$$h_l(T,x)=h_0\sum_i a_i\left(\frac{T}{T_0}-1\right)^{m_i}x^{n_i}\quad h_0=100\text{ kJ/kg},\ T_0=273.16\text{ K} \tag{B13}$$

Vapor enthalpy

$$h_g(T,y)=h_0\sum_i a_i\left(1-\frac{T}{T_0}\right)^{m_i}(1-y)^{n_i/4}\quad h_0=1000\text{ kJ/kg},\ T_0=324\text{ K} \tag{B14}$$

Coefficients of Patek equations

i	$T(p,x)$			$T(p,y)$			$y(p,x)$			$h_l(T,x)$			$h_g(T,y)$		
	m	***n***	***a***	***m***	***n***	***a***	***m***	***n***	***a***	***m***	***n***	***a***	***m***	***n***	***a***
1	0	0	+0.322302e1	0	0	+0.324004e1	0	0	+1.98022017e1	0	1	−0.761080e1	0	0	+0.128827e1
2	0	1	−0.384206e0	0	1	−0.395920e0	0	1	−1.18092669e1	0	4	+0.256905e2	1	0	+0.125247e0
3	0	2	+0.460965e−1	0	2	+0.435624e−1	0	6	+2.77479980e1	0	8	−0.247092e3	2	0	−0.208748e1
4	0	3	−0.378945e−2	0	3	−0.218943e−2	0	7	−2.88634277e1	0	9	+0.325952e3	3	0	+0.217696e1
5	0	4	+0.135610e−3	1	0	−0.143526e1	1	0	−5.91616608e1	0	12	−0.158854e3	0	2	+0.235687e1
6	1	0	+0.487755e0	1	1	+0.105256e1	2	1	+5.78091305e2	0	14	+0.619084e2	1	2	−0.886987e1
7	1	1	−0.120108e0	1	2	−0.719281e−1	2	2	−6.21736743e0	1	0	+0.114314e2	2	2	+0.102635e2
8	1	2	+0.106154e−1	2	0	+0.122362e2	3	2	−3.42198402e3	1	1	+0.118157e1	3	2	−0.237440e1
9	2	3	−0.533589e−3	2	1	− 0.224 368e1	4	3	+1.19403127e4	2	1	+0.284179e1	11	3	+0.670515e1
10	4	0	+0.785041e1	3	0	−0.201780e2	5	4	−2.45413777e4	3	3	+0.741609e1	1	3	+0.164508e2
11	5	0	−0.115941e2	3	1	+0.110834e1	6	5	+2.91591865e4	5	3	+0.891844e3	2	3	+0.936849e1
12	5	1	−0.523150e−1	4	0	+0.145399e2	7	6	−1.84782290e4	5	4	−0.161309e4	0	4	+0.842254e1
13	6	0	+0.489596e1	4	2	+0.644312e0	7	7	+2.34819434e1	5	5	+0.622106e3	1	4	−0.858807e1
14	13	1	+0.421059e−1	5	0	−0.221246e1	8	7	+4.80310617e3	6	2	−0.207588e3	0	5	−0.277049e1
15				5	2	−0.756266e0				6	4	−0.687393e1	4	6	−0.961248e0
16				6	0	−0.135529e1				8	0	+0.350716e1	2	7	+0.988009e0
17				7	2	+0.183541e0							1	10	+0.308482e0

Appendix B.3. ***Sun model*** [39]

Vapor–liquid equilibrium

$$\log P=A-\frac{B}{T}$$
$$A=7.44-1.767X+0.9823X^2+0.3627X^3$$
$$B=2013.8-2155.7X+1540.9X^2-194.7X^3 \tag{B15}$$

Liquid enthalpy	$h(T,\overline{X}) = 100\sum_{i=1}^{16} a_i\left(\frac{T}{273.16}-1\right)^{m_i}\overline{X}^{n_i}$	
	$\overline{X} = \frac{18.015X}{18.015X+17.03(1-X)}$	(B16)
VTX relation	$v(T,X) = \sum_{j=0}^{3}\sum_{i=0}^{3} a_{ij}(T-273.15)^i X^j$	(B17)

Coefficients of Eq. (B16)

i	m	n	a	i	m	n	a
1	0	1	−0.761080e1	9	2	1	+0.284179e1
2	0	4	+0.256905e2	10	3	3	+0.741609e1
3	0	8	−0.247092e3	11	5	3	+0.891844e3
4	0	9	+0.325952e3	12	5	4	−0.161309e4
5	0	12	−0.158854e3	13	5	5	+0.622106e3
6	0	14	+0.619084e2	14	6	2	−0.207588e3
7	1	0	+0.114314e2	15	6	4	−0.687393e1
8	1	1	+0.118157e1	16	8	0	+0.350716e1

Coefficients of Eq. (B17)

i	j	a_{ij}	i	j	a_{ij}	i	j	a_{ij}	i	j	a_{ij}
0	0	9.9842e−4	0	1	3.5489e−4	0	2	−1.2006e−4	0	3	3.2426e−4
1	0	−7.8161e−8	1	1	5.2261e−6	1	2	−1.0567e−5	1	3	9.8890e−6
2	0	8.7601e−9	2	1	−8.4137e−8	2	2	2.4056e−7	2	3	−1.8715e−7
3	0	−3.9076e−11	3	1	6.4816e−10	3	2	−1.9851e−9	3	3	1.7727e−9

*Standard error=4.058e−6, mean deviation=2.195e−3.

Appendix C. Properties of NH_3–$LiNO_3$

Appendix C.1. **Infante Ferreira model** [68]

VLE	$P = \exp\left(16.29+3.859(1-x)^3+\frac{-2802-4192(1-x)^3}{T+273.16}\right)$	(C1)
Enthalpy	$h = A+BT+CT^2+DT^3$ $A = \begin{cases} -215+1570(0.54-x)^2, & x \le 0.54 \\ -215+689(x-0.54)^2, & x \ge 0.54 \end{cases}$ $B = 1.15125+3.382678x$ $C = 10^{-3}(1.099+2.3965x)$ $D = 10^{-3}(3.93333x)$	(C2)
Density	$\rho = -1409.653\sqrt{x}+2046.222-1.3463T-0.0039T^2$	(C3)
Viscosity	$\eta = 10^{-6}((-5.1835T+992.337)(1-x)^{(0.08333T+6.8333)}+\exp(-0.01147T-1.744))$	(C4)
Thermal conductivity	$\lambda = 10^{-3}(2.093+4.7e-9T+(1.5478-7.612e-4T-1.5353e-5T^2)x)$	(C5)
Specific heat	$c_p = 1.15125+3.382678x+(0.002198+0.004793x)T+0.000118xT^2$	(C6)
Crystallization line	$x_c = \begin{cases} 0.3021-0.00034T-0.00000272T^2, & 0.000<x<0.2911 \\ x, & 0.2911<x<0.3000 \\ 0.3152-0.000608T, & 0.3000<x<0.3076 \\ 0.12885+0.0143T, & 0.3076<x<0.3362 \\ 0.41318-0.005402T^2, & 0.3362<x<0.4304 \\ 0.443413+0.0069T+0.000854T^2, & 0.4304<x<0.5072 \\ 0.527643-0.003126T-0.000019T^2, & 0.5072<x<0.6434 \\ 0.40761-0.004605T, & 0.6434<x<0.6649 \\ 0.57452+0.0000309T^2, & 0.6649<x<0.7826 \\ 6.7214+0.07378T, & 0.7826<x<1.0000 \end{cases}$	(C7)

Appendix C.2. ***Libotean model*** *[69,70]*

VLE	$\ln(p)=\sum_{i=0}^{3}A_i w_1^i+\frac{\sum_{i=0}^{3}B_i w_1^i}{T}$	(C8)
Density	$\rho=A+BT,\ A=\sum_{i=0}^{1}(w_1^i a_i),\ B=\sum_{i=0}^{1}(w_1^i b_i)$	(C9)
Heat capacity	$C_p=A+BT,\ A=\sum_{i=0}^{1}(w_1^i a_i),\ B=\sum_{i=0}^{1}(w_1^i b_i)$	(C10)
Viscosity	$\ln\eta=\frac{1000A}{T}+B,\ A=\sum_{i=1}^{2}(w_1^i a_i)+a_0,\ B=\sum_{i=1}^{2}(w_1^i b_i)+b_0$	(C11)

Coefficients of equation for (C8)

Coefficient	Value	Coefficient	Value
A_0/kPa	4.99×10^{0}	B_0/kPa K	-1.79×10^{3}
A_1/kPa	8.85×10^{1}	B_1/kPa K	-2.23×10^{4}
A_2/kPa	-1.98×10^{2}	B_2/kPa K	6.13×10^{4}
A_3/kPa	1.35×10^{2}	B_3/kPa K	-4.52×10^{4}

Coefficients of equation for (C9)–(C11)

Density		**Heat capacity**		**Viscosity**	
Coefficient	Value	Coefficient	Value	Coefficient	Value
a_0	1.521×10^{0}	a_0	5.593×10^{-1}	a_0	1.918
a_1	-4.528×10^{-1}	a_1	3.241×10^{0}	a_1	10.094
b_0	-1.961×10^{-5}	b_0	2.078×10^{-3}	a_2	−18.394
b_1	-1.726×10^{-3}	b_1	1.847×10^{-3}	b_0	−1.205
				b_1	−35.627
				b_2	51.529

Appendix D. Properties of NH_3–NaSCN

Appendix D.1. ***Infante Ferreira model*** *[68]*

VLE	$P=\exp\left(15.7266-0.298628x+\frac{-2548.65-2621.92(1-x)^3}{T+273.16}\right)$	(D1)
Enthalpy	$h=A+BT+CT^2+DT^3$ $A=79.72-1072x+1287.9x^2-295.67x^3$ $B=2.4081-2.2814x+7.9291x^2-3.5137x^3$ $C=10^{-2}(1.255x-4x^2+3.06x^3)$ $D=10^{-5}(-3.33x+10x^2-3.33x^3)$	(D2)
Density	$\rho=A+BT+CT^2$ $A=1707.519-2400.4348x+2256.5083x^2-930.0637x^3$ $B=-3.6341x+5.4552x^2-3.1674x^3$ $C=10^{-3}(5.1x-3.6x^2-5.4x^3)$	(D3)
Viscosity	$\eta=10^{-6}((-0.5289T+29.695)(1-X)^{(-0.0128T+3.9493)}+0.219E-10(120-T)^{4.636}+0.1)$	(D4)
Thermal conductivity	$\lambda=10^{-3}((7.655-0.0105T)(1-x)^{(-0.0075T+3.05)}+0.693E-7(T-50)^3+0.547)$	(D5)
Specific heat	$c_p=2.4081-2.2814x+7.9291x^2-3.5137x^3+(0.0251x-0.08x^2+0.0612x^3)T+(-0.0001x+0.0003x^2-0.0001x^3)T^2$	(D6)
Crystallization line	$x_c=\begin{cases}0.360207-(0.12856E-3)T-(0.30158E-5)T^2+(0.1058E-7)T^3-(0.39364E-10)T^4, & 0.000<x<0.360\\ 0.4924+0.0124T+(0.3E-3)T^2, & 0.360<x<0.430\\ 0.386-(0.94E-2)T-(1.0E-4)T^2, & 0.430<x<0.565\\ 0.2198-(0.6444E-2)T, & 0.565<x<0.735\\ 7.2395+0.080303T, & 0.735<x<1.000\end{cases}$	(D7)

Appendix D.2. ***Shrirang model*** *[72]*

VLE	$\ln(p/\text{kPa}) = A + \frac{B}{T} + C\ln\left(\frac{T}{K}\right) + D\left(\frac{T}{K}\right)^E$	(D8)
Density	$\rho/\text{kg m}^{-3} = \frac{A/\text{kg m}^{-3}}{B[1+(1-T/T_c)^D]}$	(D9)
Heat capacity	$C_p/\text{J g}^{-1}\text{K}^{-1} = A/\text{J g}^{-1}\text{K}^{-1} + (B/\text{J g}^{-1}\text{K}^{-2})\left(\frac{T}{K}\right) + (C/\text{J g}^{-1}\text{K}^{-3})\left(\frac{T}{K}\right)^2 + (D/\text{J g}^{-1}\text{K}^{-4})\left(\frac{T}{K}\right)^3 + (E/\text{J g}^{-1}\text{K}^{-5})\left(\frac{T}{K}\right)^4$	(D10)
Viscosity	$\ln(\eta/\text{mPa s}) = A + \frac{B}{(T/K)} + C\ln\left(\frac{T}{K}\right) + DT^E$	(D11)
Coefficients	$A = \sum_{i=0}^{n} a_i w_2^i,\ B = \sum_{i=0}^{n} b_i w_2^i,\ C = \sum_{i=0}^{n} c_i w_2^i,\ D = \sum_{i=0}^{n} d_i w_2^i$	(D12)

Coefficients of equation for (D8)–(D12)

Parameter	Density	Viscosity	Heat capacity	Vapor pressure
a_0	6.025725e1	1.6476e−1	6.3576e1	8.35752e1
a_1	3.638e2	−1.604e2	−1.073e2	−3.87e−2
a_2	9.692e2	−1.250e2	9.119e1	6.2386e0
a_3	0	1.144e2	0	−5.464e0
b_0	2.5443e−1	5.983e2	−9.1257e−1	−4.6697e3
b_1	8.204e−1	8.365e3	7.104e−1	3.6464e2
b_2	−2.99e−2	3.824e3	−6.662e−1	2.99e−2
b_3	0	1.800e3	0	−1.3164e3
c_0	–	−7.341e−1	5.22672e−3	−1.1607e1
c_1	–	2.373e1	−1.214e−3	−2.795e−1
c_2	–	2.064e1	1.172e−3	0
c_3	–	−2.143e1	0	0
d_0	2.888e−1	−3.7e−27	−1.32196e−5	1.7194e−2
d_1	0	0	0	0
d_2	0	0	0	0
d_3	0	0	0	0
E	–	10	1.25285e−8	1
rmsd %	0.2	1.7	1.0	2.5
δ_{max} %	0.5	4.1	2.4	7.3

T is absolute temperature, and T_c is the critical temperature of the ammonia.
δ_{max} is maximum deviation rmsd is root-mean-square deviation.

Appendix E. Properties of ternary mixtures

Appendix E.1. ***NH_3–H_2O–$LiNO_3$ (Libotean model*** *[69,70])*

VLE	$\ln(p/\text{kPa}) = \sum_{i=0}^{3} A_i w_1^i + \frac{\sum_{i=0}^{3} B_i w_1^i}{T/K},\ A = \sum_{j=0}^{2} a_{ij} w_3^j,\ B = \sum_{j=0}^{2} b_{ij} w_3^j,\quad i = 0\ldots3$	(E1)
Density	$\rho/\text{g m}^{-3} = A + B(T/K),\ A = \sum_{i=0}^{1}\left(w_1^i \sum_{j=0}^{1} a_{ij} w_3^j\right),\ B = \sum_{i=0}^{1}\left(w_1^i \sum_{j=0}^{1} b_{ij} w_3^j\right)$	(E2)
Heat capacity	$C_p/\text{J g}^{-1}\text{K}^{-1} = A + B(T/K),\ A = \sum_{i=0}^{1}(w_1^i \sum_{j=0}^{1} a_{ij} w_3^j),\ B = \sum_{i=0}^{1}(w_1^i \sum_{j=0}^{1} b_{ij} w_3^j)$	(E3)
Viscosity	$\ln(\eta/\text{mPa s}) = \frac{1000A}{T/K} + B,\ A = \sum_{i=1}^{2}\sum_{j=1}^{2}(a_{ij} w_i^j) + a_0,\ B = \sum_{i=1}^{2}\sum_{j=1}^{2}(b_{ij} w_i^j) + b_0$	(E4)

*NH_3 is component 1, $LiNO_3$ is component 2, H_2O is component 3.
Coefficients of equation for (E1)

Coefficient	**Value**	**Coefficient**	**Value**	**Coefficient**	**Value**	**Coefficient**	**Value**
a00	1.19e1	a21	−1.17e2	b00	−4.02e3	b21	2.92e4
a10	2.77e1	a31	5.48e2	b10	−2.43e3	b31	−2.65e4
a20	−8.13e1	a02	−1.64e3	b20	8.45e3	b02	−1.35e1

a30	4.66e1	a12	9.39e1	b30	−7.46e3	b12	−2.48e4
a01	−2.34e2	a22	−5.13e2	b01	2.48e4	b22	1.82e4
a11	6.93e2	a32	1.58e3	b11	−5.09e4	b32	−1.54e2

Coefficients of equation for (E2)–(E4)

Density		**Heat capacity**		**Viscosity**	
Coefficient	Value	Coefficient	Value	Coefficient	Value
a00	1.483e3	a00	2.081e0	a0	1.435
a01	4.213e2	a01	1.613e−5	a11	10.523
a10	−3.541e2	a10	3.441e−5	a12	−14.014
a11	−1.674e3	a11	1.077e−5	a21	−8.015
b00	7.859e−2	b00	−2.583e−3	a22	12.676
b01	−1.963e0	b01	8.832e−3	b0	−5.301
b10	−1.762e0	b10	1.198e−2	b11	−24.845
b11	1.594e0	b11	−6.316e−3	b12	31.503
				b21	23.013
				b22	−30.944

Appendix E.2. ***NH_3–H_2O–hydroxide (Salavera model [79])***

VLE

$$\ln(p/\mathrm{kPa}) = A_0 + A_1 m_1 + A_2 m_1^2 + A_3 m_1^3 + \frac{B_0 + B_1 m_1 + B_2 m_1^2 + B_3 m_1^3}{T/K},$$

$$A = \sum_{j=0}^{2} a_{ij} m_2^j,\ B = \sum_{j=0}^{2} b_{ij} m_2^j,\quad i = 0\ldots3$$

$$m_1 = \frac{mass_{NH_3}}{mass_{NH_3} + mass_{H_2O}} \times 100,\ m_2 = \frac{mass_{XOH}}{mass_{NH_3} + mass_{H_2O}} \times 100 \qquad \text{(E5)}$$

Density

$$\rho/\mathrm{g\ m^{-3}} = A + B(T/K) + C(T/K)^2, \qquad \text{(E6)}$$

Heat capacity

$$C_p/\mathrm{J\ g^{-1}\ K^{-1}} = A + B(T/K) + C(T/K)^2, \qquad \text{(E7)}$$

Coefficients

$$A = \sum_0^1 a_i (100w_1)^i,\ B = \sum_0^1 b_i (100w_1)^i,\ C = \sum_0^1 c_i (100w_1)^i$$

$$a_i = \sum_{j=0}^{1} a_{ij} (100w_3)^j,\ b_i = \sum_{j=0}^{1} b_{ij} (100w_3)^j,\ c_i = \sum_{j=0}^{1} c_{ij} (100w_3)^j \qquad \text{(E8)}$$

Coefficients of equation for (E5)

Coeff	**KOH**	**NaOH**	**Coeff**	**KOH**	**NaOH**
a00	1.594e1	1.724e0	b00	−4.106e3	−4.682e2
a01	1.303e−1	−2.368e−1	b01	−5.351e1	1.052e0
a02	−4.018e−3	9.744e−3	b02	1.878e0	−3.960e0
a10	6.296e1	4.500e−2	b10	1.991e−1	2.480e0
a11	−7.283e−3	5.399e−3	b11	5.437e0	−2.779e1
a12	−7.633e−5	−4.571e−4	b12	−4.441e−2	2.282e−1
a20	−1.865e−3	−4.469e−3	b20	8.730e−1	1.064e0
a21	−8.022e−5	2.311e−4	b21	−8.592e−2	−4.678e−2
a22	2.029e−5	3.082e−7	b22	−4.331e−3	−2.752e−3
a30	6.813e−6	6.574e−5	b30	−7.607e−3	−1.979e−2
a31	4.713e−6	−6.004e−6	b31	−2.839e−4	1.705e−3
a32	−4.085e−7	1.381e−7	b32	1.086e−4	−1.908e−5

Coefficients of equation for (E6)–(E8)

Coefficients for the density at 1.8 MPa								
Coeff	KOH	NaOH	Coeff	KOH	NaOH	Coeff	KOH	NaOH
a00	8.153e2	8.211e2	b00	1.393e0	1.416e0	c00	−2.803e−3	−2.856e−3

a01	1.964e1	2.338e1	b01	−5.423e−2	−6.568e−2	c01	7.521e−5	8.706e−5
a10	2.610e0	1.986e0	b10	−2.423e−2	−2.203e−2	c10	1.921e−5	1.606e−5
a11	−1.933e−1	−4.131e−2	b11	5.123e−4	−7.400e−4	c11	−8.998e−7	1.315e−6

Coefficients for the heat capacity at 1.8 MPa

Coeff	KOH	NaOH	coeff	KOH	NaOH	coeff	KOH	NaOH
a00	2.612e0	1.085e0	b00	6.676e−3	1.776e−2	c00	−7.191e−6	−2.636e−5
a01	4.297e−1	−1.716e−1	b01	−2.855e−3	7.487e−4	c01	4.364e−6	−9.297e−7
a10	1.606e−2	−8.566e−2	b10	−1.710e−4	3.920e−4	c10	4.895e−7	−2.973e−7
a11	−2.241e−2	1.921e−2	b11	1.424e−4	−1.059e−4	c11	−2.257e−7	1.452e−7

w_1 is the ammonia mass fraction, w_3 is the mass fraction of the hydroxide.

References

[1] Bogart MJP. Pitfalls in ammonia absorption refrigeration. Int J Refrig 1982;5(4):203–8.

[2] Keil C, Plura S, Radspieler M, Schweigler C. Application of customized absorption heat pumps for utilization of low-gradeheat sources. Appl Therm Eng 2008;28:2070–6.

[3] Li ZF, Sumathy K. Technology development in the solar absorption air-conditioning systems. Renew Sust Energy Rev 2000;4:267–93.

[4] Kim DS, Infante Ferreira CA. Solar refrigeration options – a state-of-the-art review. Int J Refrig 2008;31:3–15.

[5] Kalinowski P, Hwang YH, Radermacher R, Hashimi SA, Rodgers P. Application of waste heat powered absorption refrigeration system to the LNG recovery process. Int J Refrig 2009;32:687–94.

[6] Ma XH, Chen JB, Li SP, Sha QY, Liang AM, Li W, et al. Application of absorption heat transformer to recover waste heat from a synthetic rubber plant. Appl Therm Eng 2003;23:797–806.

[7] Wu SY, Eames IW. Innovations in vapour-absorption cycles. Appl Energy 2000;66:251–66.

[8] Hong DL, Tang LM, He YJ, Chen GM. A novel absorption refrigeration cycle. Appl Therm Eng 2010;30:2045–50.

[9] Herold KE, Radermacher R, Klein SA. Absorption chillers and heat pumps. Bocca Raton. CRC Press; 1996.

[10] Ahmed Y, Taha AZ. Solar air conditioning and refrigeration with absorption chillers technology in Australia – an overview on researches and applications. J Adv Sci Eng Res 2011;1:23–41.

[11] Horuz I. A comparison between ammonia–water and water–lithium bromide solutions in vapor absorption refrigeration systems. Int Commum Heat Mass 1998;25(5):711–21.

[12] Karamangil MI, Coskun S, Kaynakli O, Yamankaradeniz N. A simulation study of performance evaluation of single-stage absorption refrigeration system using conventional working fluids and alternatives. Renew Sustain Energy Rev 2010;14(7):1969–78.

[13] Muthu V, Saravanan R, Renganarayanan S. Experimental studies on R134a-DMAC hot water based vapour absorption refrigeration systems. Int J Therm Sci 2008;47:175–81.

[14] Izquierdo M, Venegas M, Rodríguez P, Lecuona A. Crystallization as a limit to develop solar air-cooled LiBr–H_2O absorption systems using low-grade heat. Sol Energy Mater Sol C 2004;81:205–16.

[15] Wang K, Abdelaziz O, Kisari P, Vineyard EA. State-of-the-art review on crystallization control technologies for water/LiBr absorption heat pumps. Int J Refrig 2011;34(6):1325–37.

[16] Yan QS, Shi WX, Tian CQ. Refrigeration technology for air conditioning. 4th ed.. Beijing: China: Architecture and Building Press; 2010 ([in Chinese]).

[17] Kang YT, Kunugi Y, Kashiwagi T. Review of advanced absorption cycles: performance improvement and temperature lift enhancement. Int J Refrig 2000;23:388–401.

[18] Srikhirin P, Aphornratana S, Chungpaibulpatana S. A review of absorption refrigeration technologies. Renew Sustain Energy Rev 2001;5:343–72.

[19] Ziegler F. State of the art in sorption heat pumping and cooling technologies. Int J Refrig 2002;25:450–9.

[20] Sun J, Fu L, Zhang SG. A review of working fluids of absorption cycles. Renew Sustain Energy Rev 2012;16:1899–906.

[21] Berlitz T, Plank H, Ziegler F, Kahn R. An ammonia–water absorption refrigerator with a large temperature lift for combined heating and cooling. Int J Refrig 1988;21(3):219–29.

[22] Blytas GC, Daniels F. Concentrated solutions of NaSCN in liquid ammonia. Solubility, density, vapor pressure, viscosity, thermal conductance, heat of solution and heat capacity. J Am Chem Soc 1962;84:1075–83.

[23] Wu W, Zhang XL, Li XT, Shi WX, Wang BL. Comparisons of different working pairs and cycles on the performance of absorption heat pump for heating and domestic hot water in cold regions. Appl Therm Eng 2012;48:349–58.

[24] Davis ROE, Olmstead LB, Landstrum FO. Vapor pressure of lithium nitrate: ammonia system. J Am Chem Soc 1921;43:1575–80.

[25] Chinnappa JCV. Experimental study of the intermittent vapour absorption refrigeration cycle employing the refrigerant–absorbent systems of ammonia water and ammonia lithium nitrate. Sol Energy 1961;5(1):1–18.

[26] Best R, Eisa MAR, Holland FA. Thermodynamic design data for absorption heat pump systems operating on ammonia–water—Part I. Cooling. Heat Recover Syst CHP 1987;7(2):167–75.

[27] Best R, Eisa MAR, Holland FA. Thermodynamic design data for absorption heat pump systems operating on ammonia–water—Part II. Heat Recover Syst CHP 1987;7(2):177–85.

[28] Best R, Eisa MAR, Holland FA. Thermodynamic design data for absorption heat pump systems operating on ammonia–water—Part III. Simultaneous cooling and heating. Heat Recover Syst CHP 1987;7(2):187–94.

[29] Best R, Eisa MAR, Holland FA. Thermodynamic design data for absorption heat transformers—III. Operating on ammonia–water. Heat Recover Syst CHP 1987;7(3):259–72.

[30] Best R, Porras L, Holland FA. Thermodynamic design data for absorption heat pump systems operating on ammonia–lithium nitrate—Part one. Cooling. Heat Recover Syst CHP 1991;11(1):49–61.

[31] Best R, Riveraa W, Pilatowsky I, Holland FA. Thermodynamic design data for absorption heat pump systems operating on ammonia–lithium nitrate—Part two. Heating. Heat Recover Syst CHP 1991;11(2–3):103–11.

[32] Best R, Riveraa W, Pilatowsky I, Holland FA. Thermodynamic design data for absorption heat pump systems operating on ammonia–lithium nitrate—Part three. Simultaneous cooling and heating. Heat Recover Syst CHP 1991;11(4):199–212.

[33] Best R, Riveraa W, Pilatowsky I, Holland FA. Thermodynamic design data for absorption heat transformers—Part four. operating on ammonia–lithium nitrate. Heat Recover Syst CHP 1990;10(5–6):539–48.

[34] Best R, Riveraa W, Hernández J, Oskam A. Thermodynamic design data for absorption heat pump systems operating on ammonia–sodium thiocyanate—I. Cooling. Heat Recovery Syst CHP 1993;13(1):1–9.

[35] Best R, Riveraa W, Hernández J, Oskam A. Thermodynamic design data for absorption heat pump systems operating on ammonia–sodium thiocyanate—III. Simultaneous cooling and heating. Heat Recover Syst CHP 1993;13(1):23–31.

[36] Best R, Riveraa W, Hernández J, Oskam A. Thermodynamic design data for absorption heat pump systems operating on ammonia–sodium thiocyanate—II. Heating. Heat Recover Syst CHP 1993;13(1):11–21.

[37] Best R, Riveraa W, Hernández J, Holland FA. Thermodynamic design data for absorption heat transformers—Part 5. Operating on ammonia–sodium thiocyanate. Heat Recover Syst CHP 1992;12(4):347–56.

[38] Antonopoulos KA, Rogdakis ED. Performance of solar-driven ammonia–lithium nitrate and ammonia–sodium thiocyanate absorption systems operating as coolers or heat pumps in Athens. Appl Therm Eng 1996;16(2):127–47.

[39] Sun DW. Comparison of the performances of NH_3–H_2O, NH_3–$LiNO_3$ and NH_3–NaSCN absorption refrigeration systems. Energy Convers Manag 1998;39(5–6):357–68.

[40] Venegas M, Izquierdo M, Vega MD, Lecuona A. Thermodynamic study of multistage absorption cycles using low-temperature heat. Int J Refrig 2002;26(8):775–91.

[41] Rivera CO, Rivera W. Modeling of an intermittent solar absorption refrigeration system operating with ammonia–lithium nitrate mixture. Sol Energy Mater Sol C 2003;76(3):417–27.

[42] Zhu LH, Gu JJ. Second law-based thermodynamic analysis of ammonia/sodium thiocyanate absorption system. Renew Energy 2010;35:1940–6.

[43] Rivera W, Best R. Boiling heat transfer coefficients inside a vertical smooth tube for water/ammonia and ammonia/lithium nitrate mixtures. Int J Heat Mass Transf 1999;42:905–21.

[44] Heardand CL, Ayala R. Carbon and stainless steel in solutions of lithium nitrate in ammonia at moderate temperatures. Mater Corros 2003;54:609–11.

[45] Mclinden M, Radermacher R. An experimental comparison of ammonia–water and ammonia–water–lithium bromide mixtures in an absorption heat pump. ASHRAE Transf 1985;91(2):1837–46.

[46] Ahlby L, Hodgett D, Radermacher R. NH_3–H_2O–LiBr as working fluid for the compression/absorption cycle. Int J Refrig 1993;16(4):265–73.

[47] Wu TH, Wu YY, Yu ZQ, Zhao HC, Wu HL. Experimental investigation on an ammonia–water–lithium bromide absorption refrigeration system without solution pump. Energy Convers Manag 2011;52:2314–9.
[48] Oronel C, Amaris C, Vallès M, Bourouis M. Experiments on the characteristics of saturated boiling heat transfer in a plate heat exchanger for ammonia/lithium nitrate and ammonia/(lithium nitrate+water). Thermal issues in emerging technologies, ThETA 3, Cairo; 2010.
[49] Bokelmann H. Presentation of new working fluids for absorption heat pumps. Paris: Absorption Heat Pump Congress; 1985.
[50] Reiner RH, Zaltash A. Evaluation of ternary ammonia water fluids for GAX and regenerative absorption cycles. Report ORNL/CF-91/263; 1991.
[51] Sathyabhama A. Effect of salt on boiling heat transfer of ammonia–water mixture. Heat Mass Transf 2012;48:497–503.
[52] Reiner RH, Zaltash A. Corrosion screening of potential fluids for ammonia-water absorption cycles. Report ORNL/CF-92/41; 1992.
[53] Reiner RH, Zaltash A. Densities and viscosities of ternary ammoniawater fluids. ASME winter annual meeting; 1993.
[54] Steiu S, Salavera D, Bruno JC, Coronas A. A basis for the development of new ammonia–water–sodium hydroxide absorption chillers. Int J Refrig 2009;32(4):577–87.
[55] Balamuru VG, Ibrahim OM, Barnett SM. Simulation of ternary ammonia–water–salt absorption refrigeration cycles. Int J Refrig 2000;23:31–42.
[56] Steiu S, Bruno JC, Coronas A, Roman MFS, Ortiz I. Separation of Ammonia/water/sodium hydroxide mixtures using reverse osmosis membranes for low temperature driven absorption chillers. Ind Eng Chem Res 2008;47:10020–6.
[57] Lemmon E, Huber M, McLinden M. NIST reference fluid thermodynamic and transport properties REFPROP 8. NIST standard reference database 23; 2007.
[58] F-Chart software. Engineering equation solver see also. Academic version 6.867-3D. Madison, USA; 2003.
[59] Cleland AC. Computer subroutines for rapid evaluation of refrigerant thermodynamic properties. Int J Refrig 1986;9(6):346–51.
[60] ASHRAE. ASHRAE handbook, Fundamentals. Atlanta, U.S.A; 1993.
[61] El-Shaarawi MAI, Al-Nimr MA. Equations for use with computers to evaluate the performance of NH_3–H_2O intermittent solar refrigerators. Energy Convers Manag 1990;30(3):315–27.
[62] Shulz S. Equations on state for the system ammonia–water for use with computers. IIR, Meeting Comission II, Washington; 1971.
[63] Ziegler B, Trepp T. Equation of state for ammonia–water mixtures. Int J Refrig 1984;7(2):101–6.
[64] Yokozeki A. Theoretical performances of various refrigerant–absorbent pairs in a vapor-absorption refrigeration cycle by the use of equations of state. Appl Energy 2005;80:383–99.
[65] Mejbri K, Bellagi A. Modelling of the thermodynamic properties of the water–ammonia mixture by three different approaches. Int J Refrig 2006;29:211–8.
[66] Patek J, Klomfar J. Simple functions for fast calculations of selected thermodynamic properties of the ammonia–water system. Int J Refrig 1995;18(4):228–34.
[67] Aggarwal MK, Agarwal RS. Thermodynamic properties of lithium nitrate ammonia mixtures. Int J Energy Res 1986;10(1):59–68.
[68] Infante Ferreira CA. Thermodynamic and physical property data equations for ammonia–lithium nitrate and ammonia–sodium thiocyanate solutions. Sol Energy 1984;32(2):231–6.
[69] Libotean S, Salavera D, Valles M, Esteve X, Coronas A. Vapor liquid equilibrium of ammonia+lithium nitrate+water and ammonia+lithium nitrate solutions from (293.15 to 353.15)K. J Chem Eng Data 2007;52:1050–5.
[70] Libotean S, Martin A, Salavera D, Valles M, Esteve X, Coronas A. Densities, viscosities, and heat capacities of ammonia+lithium nitrate and ammonia+lithium nitrate+water solutions between (293.15 and 353.15)K. J Chem Eng Data 2008;53:2383–8.
[71] Rogdakis ED, Antonopoulos KA. Thermodynamic cycle, correlations and nomograph for NH_3–NaSCN absorption refrigeration systems. Heat Recover Syst CHP 1995;15(6):591–9.
[72] Chaudhari SK, Salavera D, Coronas A. Densities, viscosities, heat capacities, and vapor-liquid equilibria of ammonia+sodium thiocyanate solutions at several temperatures. J Chem Eng Data 2011;56:2861–9.
[73] Peters R, Grab O, Korinth C, et al. Vapor–liquid equilibrium in the system $NH_3+H_2O+LiBr$. 1. Measurements at $T=303$–423 K and $p=0.1$–1.5 MPa. J Chem Eng Data 1995;40(4):769–74.
[74] Peters R, Korinth C, Keller JU. Vapor–liquid equilibrium in the system $NH_3+H_2O+LiBr$. 2. Data correlation. J Chem Eng Data 1995;40(4):775–83.
[75] Peters R, Busse R, Keller JU. Solid–liquid equilibria in the systems NH_3–H_20–LiBr and H_20–LiBr at $p=1$ atm in the range from -35 to $80\,^{\circ}C$. Int J Thermophys 1993;14(4):763–75.
[76] Wu YY, Chen Y, Wu TH. Experimental researches on characteristics of vapor–liquid equilibrium of NH_3–H_2O–LiBr system. Int J Refrig 2006;29(2):328–35.
[77] Aspen Technology, Inc. Ten Canal Park, Cambridge, Massachusetts 02141-2200 USA.
[78] Brass M, Pritzel T, Schulte E, Keller JU. Measurements of vapor–liquid equilibria in the systems NH_3–H_2O–NaOH and NH_3–H_2O–KOH at temperatures of 303 and 318 K and pressures $0.1\ MPa < p < 1.3$ MPa. Int J Thermophys 2000;21(4):883–98.
[79] Salavera D, Chaudhari SK, Esteve X, Coronas A. Vapor liquid equilibria of ammonia+water+potassium hydroxide and ammonia+water+sodium hydroxide solutions at temperatures from (293.15 to 353.15)K. J Chem Eng Data 2005;50:471–6.
[80] Salavera D, Libotean S, Patil KR, Esteve X, Coronas A. Densities and heat capacities of the ammonia+water+NaOH and ammonia+water+KOH solutions. J Chem Eng Data 2006;51:1020–5.
[81] Lazzarin RM, Gasparella A, Longo GA. Ammonia–water absorption machines for refrigeration: theoretical and real performances. Int J Refrig 1996;19(4):239–46.
[82] Clerx M, Trezek GJ. Performance of an aqua-ammonia absorption solar refrigerator at sub-freezing evaporator conditions. Sol Energy 1987;39(5):379–89.
[83] Moreno-Quintanar G, Rivera W, Best R. Comparison of the experimental evaluation of a solar intermittent refrigeration system for ice production operating with the mixtures $NH_3/LiNO_3$and $NH_3/LiNO_3/H_2O$. Renew Energy 2012;38:62–8.
[84] Colonna P, Gabrielli S. Industrial trigeneration using ammonia–water absorption refrigeration systems (AAR). Appl Therm Eng 2003;23(4):381–96.
[85] Bassols J, Kuckelkorn B, Langreck J, Schneider R, Veelken H. Trigeneration in the food industry. Appl Therm Eng 2002;22(6):595–602.
[86] He YJ, Chen GM. Experimental study on an absorption refrigeration system at low temperatures. Int J Therm Sci 2007;46:294–9.
[87] Kaushik SC, Kumar R. Computer-aided conceptual thermodynamic design of a two-stage dual fluid absorption cycle for solar refrigeration. Sol Energy 1985;35(5):401–7.
[88] Kaushik SC, Kumar R, Chandra S. Thermal modelling and parametric study of two stage absorption refrigeration and air-conditioning systems. Int J Energy Res 1985;9(4):391–402.
[89] Kaushik SC, Kumar R. Thermodynamic study of a two-stage vapour absorption refrigeration system using NH_3 refrigerant with liquid/solid absorbents. Energy Convers Manag 1985;25(4):427–31.
[90] Rogdakis ED, Antonopoulos KA. Performance of a low-temperature NH_3–H_2O absorption–refrigeration system. Energy 1992;17(5):477–84.
[91] Fernández-Seara J, Sieres J, Vázquez M. Compression–absorption cascade refrigeration system. Appl Therm Eng 2006;26(5–6):502–12.
[92] Arivazhagan S, Saravanan R, Renganarayanan S. Experimental studies on HFC based two-stage half effect vapour absorption cooling system. Appl Therm Eng 2006;26:1455–62.
[93] Arzoz D, Venegas M, Rodriguez P. Solar absorption refrigeration cycle using $LiNO_3$–NH_3 solution and flat plate collectors. In: Proceedings of the international sorption heat pump conference. Shanghai, China; 2002.
[94] Kumar AR, Udayakumar M. Studies of compressor pressure ratio effect on GAXAC (generator–absorber–exchange absorption compression) cooler. Appl Energy 2008;85(12):1163–72.
[95] Kumar AR, Udayakumar M. Simulation studies on GAX absorption compression cooler. Energy Convers Manag 2007;48:2604–10.
[96] Kang YT, Hong H, Park KS. Performance analysis of advanced hybrid GAX cycles: HGAX. Int J Refrig 2004;27:442–8.
[97] Pratihar AK, Kaushik SC, Agarwal RS. Performance evaluation of a small capacity compression–absorption refrigeration system. Appl Therm Eng 2012;42:41–8.
[98] Hultén M, Berntsson T. The compression/absorption cycle – influence of some major parameters on COP and a comparison with the compression cycle. Int J Refrig 1999;22:91–106.
[99] Morawetz E. Sorption–compression heat pumps. Int J Energy Res 1989;13(1):83–102.
[100] Zhou Q, Radermacher R. Development of a vapour compression cycle with a solution circuit and desorber/absorber heat exchange. Int J Refrig 1997;20(2):85–95.
[101] Tariquea SM, Siddiqui MA. Performance and economic study of the combined absorption/compression heat pump. Energy Convers Manag 1999;40(6):575–91.
[102] Hultén M, Berntsson T. The compression/absorption heat pump cycle—conceptual design improvements and comparisons with the compression cycle. Int J Refrig 2002;25(4):487–97.
[103] Li XT, Wu W, Zhang XL, Shi WX, Wang BL. Energy saving potential of low temperature hot water system based on air source absorption heat pump. Appl Therm Eng 2012;48:317–24.
[104] 〈http://www.robur.com/〉.
[105] Wu W, Wang BL, You T, Shi WX, Li XT. A potential solution for thermal imbalance of ground source heat pump systems in cold regions: ground source absorption heat pump. Renew Energy 2013;59:39–48.
[106] Wu W, Zhang XL, You T, Li XT, Shi WX, Wang BL. Analysis on heating performance of ground source absorption heat pump system with direct cooling in summer. In: Proceedings of the second international conference on building energy and environment. Colorado, USA; 2012.
[107] Wilbur PJ, Mancini TR. A comparison of solar absorption air-conditioning systems. Sol Energy 1976;18:569–76.
[108] Karakas A, Egrican N, Uygur S. Second-law analysis of solar absorption–cooling cycles using lithium bromide/water and ammonia/water as working fluids. Appl Energy 1990;37:169–87.
[109] Swartman RK, Ha V, Swaminathan C. Comparison of ammonia–water and ammonia–sodium thiocyanate as the refrigerant–absorbent in a solar refrigeration system. Sol Energy 1975;17(2):123–7.
[110] Staicovici MD. An autonomous solar ammonia–water refrigeration system. Sol Energy 1986;36:115–24.
[111] El-Shaarawi MAI, Said SAM, Siddiqui MU. New simplified correlations for aqua-ammonia intermittent solar-powered absorption refrigeration systems. Int J Air-Cond Refrig 2012;20(2):1–13, http://dx.doi.org/10.1142/S2010132512500083.
[112] Sierra FZ, Best R, Holland FA. Experiments on an absorption refrigeration system powered by a solar pond. Heat Recover Syst CHP 1993;13:401–8.

[113] Hernández JA, Rivera W, Colorado D, Moreno-Quintanar G. Optimal COP prediction of a solar intermittent refrigeration system for ice production by means of direct and inverse artificial neural networks. Sol Energy 2012;86(4):1108–17.
[114] Li ZF, Sumathy K. Technology development in the solar absorption air-conditioning systems. Renew Sustain Energy Rev 2000;4:267–93.
[115] AliMansoori G, Patel V. Thermodynamic basis for the choice of working fluids for solar absorption cooling systems. Sol Energy 1979;22:483–91.
[116] Shiran Y, Shitzer A, Degani D. Computerized design and economic evaluation of an aqua-ammonia solar operated absorption system. Sol Energy 1982;29:43–54.
[117] Uppal AH, Norton B, Probert SD. A low-cost solar-energy stimulated absorption refrigerator for vaccine storage. Appl Energy 1986;25:167–74.
[118] Kouremenos DA, Antonopoulos KA, Rogdakis ED. Performance of solar NH_3/H_2O absorption cycle in the Athens area. Sol Energy 1985;35(3):259–69.
[119] Alvares SG, Trepp C. Simulation of a solar driven aqua-ammonia absorption refrigeration system Part 1: mathematical description and system optimization. Int J Refrig 1987;10:40–8.
[120] Kouremenos DA. A tutorial on reversed NH_3–H_2O absorption cycles for solar applications. Sol Energy 1985;34(1):101–15.
[121] Hammad M, Habali S. Design and performance study of a solar energy powered vaccine cabinet. Appl Therm Eng 2000;20:1785–98.
[122] Francisco AD, Illanes R, Torres JL, Castillo M, Blas AD, Prieto E, et al. Development and testing of a prototype of low-power water–ammonia absorption equipment for solar energy applications. Renew Energy 2002;25(4):537–44.
[123] Mendes LF, Collares-Pereira M, Ziegler F. A rich solution spray as a refining method in a small capacity, single effect, solar assisted absorption machine with the pair NH_3/H_2O: experimental results. Energy Convers Manag 2007;48(11):2996–3000.
[124] Abdulateef JM, Sopian K, Alghoul MA. Optimum design for solar absorption refrigeration systems and comparison of the performances using ammonia–water, ammonia–lithium nitrate and ammonia–sodium thiocyanate solutions. Int J Mech Mater Eng 2008;3(1):17–24.
[125] Abu-Ein SQ, Fayyad SM, Momani W, Al-Bousoul M. Performance analysis of solar powered absorption refrigeration system. Heat Mass Transf 2009;46(2):137–45.
[126] Kaushik SC, Kumar R. A comparative study of an absorber heat recovery cycle for solar refrigeration using NH_3-refrigerant with liquid/solid absorbents. Int J Energy Res 1987;11(1):123–32.
[127] Jawahar CP, Saravanan R. Generator absorber heat exchange based absorption cycle—a review. Renew Sustain Energy Rev 2010;14:2372–82.
[128] Ahachad M, Charia M, Bernatchou A. Solar absorption heat transformer applications to absorption refrigerating machines. Int J Energy Res 1993;17(8):719–26.
[129] Kouremenos DA, Antonopoulos KA, Rogdakis E. Performance of a solar driven compound NH_3/H_2O–H_2O/LiBr absorption refrigeration system in Athens. Sol Wind Technol 1990;7(6):685–97.
[130] Lee KR, Kim SS, Kang YT. Development of binary nanoemulsion to apply for diffusion absorption refrigerator as a refrigerant. In: Proceedings of the 6th Asian conference on refrigeration and air conditioning, Xi'an, China; 2012.
[131] Jakob U, Eicker U. Solar cooling with diffusion absorption principle. Cologne, German: World Renewable Energy Congress VII; 2002.
[132] Wang HDA. New style solar-driven diffusion absorption refrigerator and its operating characteristics. Energy Procedia 2012;18:681–92.
[133] Ventas R, Lecuona A, Zacarías A, Venegas M. Ammonia–lithium nitrate absorption chiller with an integrated low-pressure compression booster cycle for low driving temperatures. Appl Therm Eng 2010;30(11–12):1351–9.
[134] Ventas R, Vereda C, Lecuona A, Venegas M. Experimental study of a thermochemical compressor for an absorption/compression hybrid cycle. Appl Energy 2012;97:297–304.
[135] Best R, Heard CL, Fernández H, Siqueiros J. Developments in geothermal energy in Mexico-Part five: the commissioning of an ammonia/water absorption cooler operating on low enthalpy geothermal energy. J Heat Recover Syst 1986;6(3):209–16.
[136] Best R, Heard CL, Peña P, Fernández H, Holland FA. Developments in geothermal energy in Mexico—Part twenty six: experimental assessment of an ammonia/water absorption cooler operating on low enthalpy geothermal energy. Heat Recover Syst CHP 1990;10(1):61–70.
[137] Ayala R, Frías JL, Lam L, Heard CL, Holland FA. Experimental assessment of an ammonia/lithium nitrate absorption cooler operated on low temperature geothermal energy. Heat Recover Syst CHP 1994;14(4):437–46.
[138] Kairouani L, Nehdi E. Thermodynamic analysis of an absorption/compression refrigeration system using geothermal energy. Am J Appl Sci 2005;2(5):914–9.
[139] Kairouani L, Nehdi E. Cooling performance and energy saving of a compression–absorption refrigeration system assisted by geothermal energy. Appl Therm Eng 2006;26(2–3):288–94.
[140] Kairouani L, Nehdi E, Iffa RB. Thermodynamic investigation of two-stage absorption refrigeration system connected by a compressor. Am J Appl Sci 2005;2(6):1036–41.
[141] Siddiqui MA. Optimum generator temperatures in four absorption cycles using different sources of energy. Energy Convers Manag Vol 1993;34(4):251–66.
[142] Villela IAC, Silveira JL. Thermoeconomic analysis applied in cold water production system using biogas combustion. Appl Therm Eng 2005;25(8–9):1141–52.
[143] Huang Y, Wang YD, Rezvani S, McIlveen-Wright DR, Anderson M, Hewitt NJ. Biomass fuelled trigeneration system in selected buildings. Energy Convers Manag 2011;52(6):2448–54.
[144] Fernández-Seara J, Vales A, Vázquez M. Heat recovery system to power an onboard NH_3–H_2O absorption refrigeration plant in trawler chiller fishing vessels. Appl Therm Eng 1998;18(12):1189–205.
[145] Erickson DC, Anand G, Papar, RA,Tang J. Refinery waste heat powered absorption refrigeration-cycle specification and design. In: Proceedings of the 1998 ASME international mechanical engineering congress and exposition, Anaheim, USA; 1998.
[146] Kalinowski P, Hwang YH, Radermacher R, Hashimi SA, Rodgers P. Application of waste heat powered absorption refrigeration system to the LNG recovery process. Int J Refrig 2009;32(4):687–94.
[147] Somers CM. Simulation of absorption cycles for integration into refining processes. Thesis, University of Maryland. ⟨http://hdl.handle.net/1903/9394⟩; 2009.
[148] Kang YT, Akisawa A, Kashiwagi T. An advanced GAX cycle for waste heat recovery: WGAX cycle. Appl Therm Eng 1999;19(9):933–47.
[149] Yang QC, Zhang XL, Wang X, et al. Review on absorption thermal energy storage technologies (in Chinese). Chin Sci Bull 2011;56:669–78.
[150] Rizza JJ. Ammonia–water low-temperature thermal storage system. J Sol Energy Eng 1998;120:25–31.
[151] Mugnier D, Goetz V. Energy storage comparison of sorption systems for cooling and refrigeration. Sol Energy 2001;71(1):47–55.
[152] Liu H, N'Tsoukpoe KE, Le Pierres N, Luo L. Evaluation of a seasonal storage system of solar energy for house heating using different absorption couples. Energy Convers Manag 2011;52:2427–36.
[153] Wang RZ, Ge TS, Chen CJ, Ma Q, Xiong ZQ. Solar sorption cooling systems for residential applications: options and guidelines. Int J Refrig 2009;32(4):638–60.
[154] Oronel C, Amaris C, Bourouis M, Vallès M. Heat and mass transfer in a bubble plate absorber with NH_3/$LiNO_3$ and NH_3/($LiNO_3$+H_2O) mixtures. Int J Therm Sci 2013;63:105–14.
[155] Velázquez N, Best R. Methodology for the energy analysis of an air cooled GAX absorption heat pump operated by natural gas and solar energy. Appl Therm Eng 2002;22(10):1089–103.
[156] De Francisco A, Illanes R, Torres JL, Castillo M, De Blas M, Prieto E, et al. Development and testing of a prototype of low-power water–ammonia absorption equipment for solar energy applications. Renew Energy 2002;25:537–44.
[157] Lin P, Wang RZ, Xia ZZ. Numerical investigation of a two-stage air-cooled absorption refrigeration system for solar cooling: cycle analysis and absorption cooling performances. Renew Energy 2011;36(5):1401–12.
[158] Du S, Wang RZ, Lin P, Xu ZZ, Pan QW, Xu SC. Experimental studies on an air-cooled two-stage NH_3–H_2O solar absorption air-conditioning prototype. Energy 2012;45(1):581–7.
[159] Jakob U, Pink W. Development and investigation of an ammonia/water absorption chiller – chilli®PSC–for a solar cooling system. In: Proceedings of the 2nd international conference solar air-conditioning, Tarragona, Spain; 2007.
[160] Häberle A, Luginsland F, Zahler C, Berger M, Rommel M, Henning HM, et al. A linear concentrating Fresnel collector driving a NH_3–H_2O absorption chiller. In: Proceedings of the 2nd international conference solar air-conditioning, Tarragona, Spain; 2007.
[161] Wang Handong. Experimental study on $LiNO_3$–NH_3 diffusion–absorption refrigeration system. Key Eng Mater 2011;474–476:2335–40.
[162] Omar Abdullah Mohammad, Chung Hieng Tang. Comparative analysis of performance and techno-economics for a H_2O–NH_3–H_2 absorption refrigerator driven by different energy sources. Appl Energy 2010;87(5):1535–45.
[163] Liu ZB, Hao YT, Liu T. Numerical simulation and experimental investigation of NaSCN–NH_3 diffusion absorption refrigeration system. Asia-Pacific: Power and Energy Engineering Conference (APPEEC); 2010.
[164] Chan CY, Haselden GG. Computer-based refrigerant thermodynamic properties, Part 1: basic equations. Int J Refrig 1981;4(1):7–12.